Feasibility study for a novel instrumental technique to characterize subsurface currents and hydrography within the Alaska OCS

Principal Investigator: Kay McMonigal[1]

Collaborators: Jacyln Beight[1]

[1] College of Fisheries and Ocean Sciences, University of Alaska Fairbanks

April 2025
Final Report
OCS Study BOEM 2025-018

Contact Information:
Email: uaf-cmi@alaska.edu
CFOS Research Homepage: https://www.uaf.edu/cfos/research/cmi

This study was funded by the University of Alaska Coastal Marine Institute and the U.S. Department of the Interior, Bureau of Ocean Energy Management Alaska OCS Region (cooperative agreement M19AC00020). This report, OCS Study BOEM 2025-018, is available electronically from https://www.boem.gov/akpubs

Citation: McMonigal K., Beight, J. 2025. Feasibility study for a novel instrumental technique to characterize subsurface currents and hydrography within the Alaska OCS. Final Report, OCS Study BOEM 2025-018, University of Alaska Coastal Marine Institute and USDOI, BOEM Alaska OCS Region. 53 p. Contract No.: M23AC00011.

Contents

List of Figures

List of Tables

List of Abbreviations and Acronyms

ACC	Alaska Coastal Current
ADCP	Acoustic Doppler current profiler
BOEM	Bureau of Ocean Energy Management
CPIES	Current and pressure-recording inverted echosounder
GEM	Gravest empirical mode
NGA-LTER	Northern Gulf of Alaska Long Term Ecological Research
OCS	Outer continental shelf
ROMS	Regional ocean modeling system
WOD	World ocean database

1 Background

Ocean circulation within the Alaska Outer Continental Shelf (OCS) is important for the regionally productive Alaska Marine ecosystem (Coyle et al., 2008; Dunton et al., 2006), but also mediates the dispersal of ocean pollutants such as oil spills (Royer et al., 1990). While some aspects of the flow can be monitored from the ocean surface, subsurface data is essential for adequately constraining drivers of ecosystem changes, such as transport of nutrients and zooplankton, for understanding possible risks associated with marine mineral extraction, and for planning spill responses to ocean-borne contaminant releases. The Alaska OCS regional circulation has changed over recent decades: notably, the Bering Strait volume has increased by about 25% (Woodgate, 2018; Peralta-Ferriz & Woodgate, 2023) and coastal upwelling conditions have suppressed circulation in the Gulf of Alaska (Rallu De Malibra et al. 2024). This change in the Bering Strait flow implies that there are likely changes to the flow up- and down-stream of the Strait, due to volume conservation. The structure of these changes is largely unknown, and different circulations are likely associated with different drivers and fates of ocean-borne materials. For instance, despite the volume transport increase in the Bering Strait, no change has been observed in the Alaska Coastal Current (ACC). This suggests different dynamical drivers of these currents, and possibly complex changes to circulation and water masse exchanges across the ACC front and as far downstream as the western Beaufort Sea shelf. It is likely that the controls on the circulation vary by timescale and season (Danielson et al., 2014; Woodgate, 2018).

To better constrain our understanding of current and potential future changes to ocean circulation in the Alaska OCS, seasonal timeseries of subsurface data of ocean currents and water masses (assessed by temperature and salinity) are needed. Ocean circulation model data (e.g., Curchitser et al., 2018; Daniels et al., 2016) can be used as input for oil spill trajectory models, however, more observational data are needed to ensure model fidelity under a changing climate. A possible novel observational technique to obtain such data are bottom mounted Current and Pressure Recording Inverted Echosounders (CPIES), which are manufactured by University of Rhode Island. CPIES measure acoustic travel time and near bottom absolute velocities, from which temperature, salinity, and current velocity profiles can be estimated.

Typical uses of CPIES include estimating heat and freshwater transport of currents (McMonigal et al., 2020, 2022), quantifying heat transport by mesoscale eddies (Bishop, 2013; Donohue et al., 2010), and assessing trends in bottom temperatures (Meinen et al., 2020). CPIES deployed in oceans with sea-ice cover can detect the presence and thickness of ice (Andres et al., 2015; Sanchez et al., 2021). Compared to other kinds of bottom mounted moorings, CPIES can be cheaper and easier to deploy. Typically, to resolve temperature, salinity, and current velocities of the full water column, multiple instruments would be deployed at different depths on a mooring. This can quickly expand the cost of instrumentation, batteries, and calibrations. In contrast, CPIES are a single instrument which can estimate full depth profiles of temperature, salinity, and current velocities. Additionally, CPIES are relatively lightweight and do not require the amount of flotation or anchors of a mooring with many instruments. This makes deployment and retrieval easier and faster.

Data collected from CPIES, which is an active acoustic instrument, can estimate the temperature and salinity profile of a water column by taking advantage of the relationship between sound speed and water density. Temperature and Salinity are the two variables with the

highest influence on underwater sound (Figure 1) and this instrument has been tested reliably in water with a depth of >500m, where the total acoustic travel time to the surface and back is near or exceeding 1 sec. However, the same principles apply in shallower shelf regions and recent modifications to the CPIES firmware has enabled deployment in about 150 m water depth in the Florida Straits (personal communication, Lisa Beal). Prior to deploying CPIES in shelf regions, the signal-to-noise ratio of acoustic travel time needs to be estimated to ensure this method is adaptable to the region and to determine the ideal deployment locations. This study focuses on identifying whether, and where, CPIES could be deployed to estimate temperature, salinity, and velocity magnitude within the Alaska OCS.

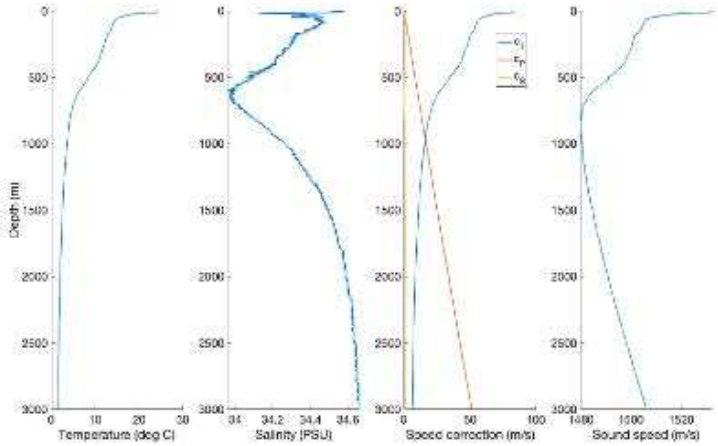

Figure 1. Profiles of temperature, salinity, sound speed correction due to temperature, pressure, and salinity, and total sound speed for a profile located at 35.6°N, 172.5°W in the Pacific Ocean.

2 Objectives and Hypotheses

Our objectives are to:

- Determine the feasibility of using CPIES to measure ocean temperature, salinity, and currents on the Beaufort Sea shelf
- Determine the feasibility of using CPIES to measure ocean temperature, salinity, and currents in Lower Cook Inlet

We hypothesize that CPIES will be able to estimate temperature with low errors, due to the strong relationship between temperature and the speed of sound (Figure 2). Further, we hypothesize that CPIES will be able to estimate currents in waters deeper than 500 m, as this is well established in other regions.

3 Methods

We assess the feasibility (using signal-to-noise ratios) and errors in using CPIES to estimate measure temperature, salinity, and velocity using the Regional Ocan Modeling System model (ROMS) described in Curchitser et al. 2018 and Danielson et al. 2016. We do this in two ways: first, we use signal-to-noise ratios of round trip acoustic travel time to assess whether it is possible that CPIES may produce reasonable estimates. Secondly, we compare temperature,

salinity, and current velocity magnitude from the ROMS model (referred to as "Model truth") to estimates of temperature, salinity, and current velocity magnitude derived only from the speed of sound from the ROMS model run through the "gravest empirical mode" (GEM) method (Donohue et al. 2010). This can be described as "simulating" CPIES within the ROMS model, where we can compare the model truth to the "GEM estimated" values to derive an error. We hypothesized that error may depend on bottom depth and so we select locations with varying bottom depths. Next, data of temperature, salinity, and current velocities are selected from ROMS using python scripts subset_TS.py and subset_velocity.py. For the Beaufort Sea shelf, data were selected at the five colored dots shown on Figure 2. This was conducted on University of Alaska Fairbank's high performance computing system, Chinook. These files were then downloaded to the researcher's local computer and read into Matlab using calculate_travel_time.m. This provides measures of central tendency on expected signal-to-noise ratios. To test whether the acoustic travel time can yield acceptable estimates of temperature and salinity, a GEM is estimated using CTD (conductivity, temperature and depth) data from the World Ocean Database (WOD), using CreateGEMBeaufort.m and mkGEM_Beaufort.m. The GEM is applied using the model acoustic travel times and compared to the ROMS data T and S using tau_index_to_TSV.m. In Lower Cook Inlet and Shelikof Strait, very few CTD profiles were available through the WOD. To supplement the available profiles, we added data from the Northern Gulf of Alaska Long Term Ecological Research project. There is work towards recovering historical CTD profiles from Lower Cook Inlet and adding them to WOD (BOEM 2025), however, such work will not be completed by the end the project.

The anticipated instrumental error for 20-hour low pass filtered estimates is (2.2 ms)$(24*20)^{(-1/2)}$ = 0.1 ms = $1x10^{-4}$ s, where the multiplier of 24 comes from 24 pings per hour (Donohue et al. 2010). This low pass filter is chosen to filter out most tidal variability, which CPIES would not necessarily be expected to resolve. Thus, for CPIES signal-to-noise ratio to be above 1, the standard deviation of 20-hour low pass filtered acoustic travel time must be at least $1x10^{-4}$ s. Recent upgrades to the CPIES firmware can increase the instrument's sampling rate to 72 pings per hour (personal communication, Randy Watts), lowering the error to (2.2 ms)$(72*20)^{(-1/2)}$ = 0.06 ms = $6x10^{-5}$ s.

To estimate errors in CPIES measurements of velocity, we use the GEM temperature and salinity to calculate specific volume anomaly. This is then converted into a baroclinic velocity profile using the equations:

$$u_{baroclinic} = -\frac{1}{f}\frac{\partial}{\partial y}\int_{p}^{p_{ref}} [\alpha(35,0,p) - \alpha(S,T,p)]\, dp$$

$$v_{baroclinic} = \frac{1}{f}\frac{\partial}{\partial x}\int_{p}^{p_{ref}} [\alpha(35,0,p) - \alpha(S,T,p)]\, dp$$

Where f is the Coriolis force, p is pressure, α is specific volume anomaly at a given temperature, salinity, and pressure. The derivatives are calculated using finite centered differences between model grid points. Similar to the temperature and salinity analysis, the baroclinic velocity from the GEM method is compared to baroclinic velocity from the ROMS model.

4 Beaufort Sea Shelf

For the Beaufort analysis, 5 locations along a line perpendicular to the coast are chosen (Figure 2). These shelf locations were chosen to span a range of bottom depths, because bottom

depth is hypothesized to play a dominant role in the signal-to-noise ratio. We generally expect that other locations along the Beaufort Sea shelf away from topographic features such as Barrow Canyon would yield similar results, because temperature and salinity are related to water masses which are consistent throughout the region.

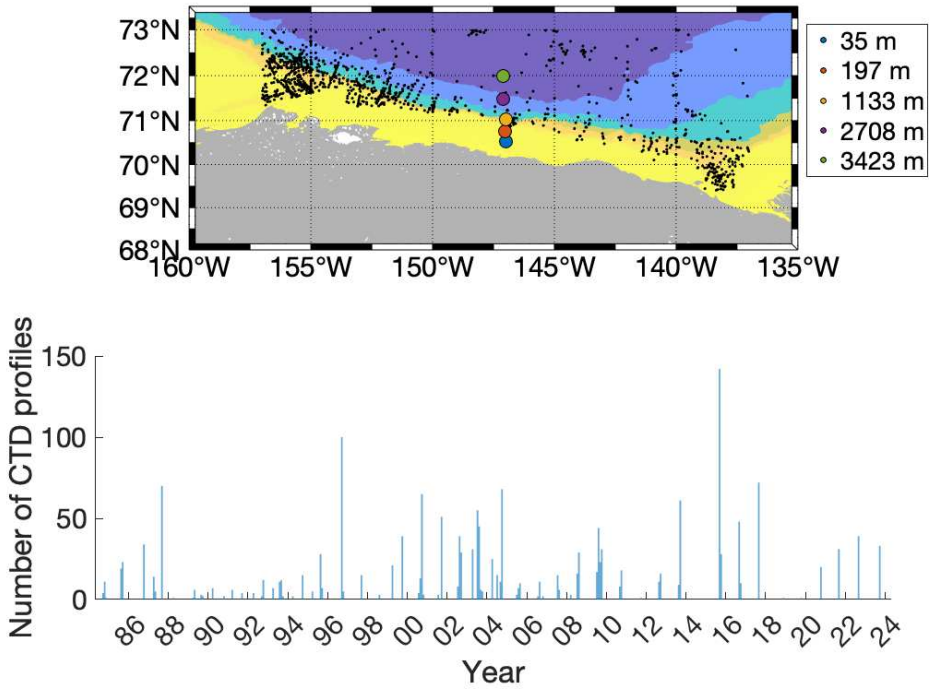

Figure 2. Locations where CPIES feasibility has been assessed, on the Beaufort Sea shelf and slope. Black dots show locations of CTD observations in the region from the World Ocean Database. Bottom panel shows distribution of CTD observations in time.

4.1 Signal-to-noise ratios over the Beaufort Sea shelf (back to contents)

The standard deviation of the low pass filtered acoustic travel times across the Beaufort Sea shelf are shown in Table 1. Surprisingly, signal-to-noise ratios are highest at the mid-depth locations (197m and 1133m). This appears to be because, even though the mid-depth locations are shallower, they have more variability in temperatures and salinities than the offshore locations (Figure 3).

Table 1. Signal-to-noise ratios on Beaufort Sea shelf.

Longitude	Latitude	Depth	Travel time standard deviation (s)	S/N ratio with standard sample rate	S/N ratio with increased sample rate
147°W	70.5°N	**35 m**	9.30×10^{-5}	0.9	1.6
147°W	70.75°N	**197 m**	4.10×10^{-4}	4.1	6.8
147°W	71°N	**1133 m**	5.82×10^{-4}	5.8	9.7
147°W	71.5°N	**2708 m**	2.04×10^{-4}	2.0	3.4
147°W	72°N	**3423 m**	2.03×10^{-4}	2.0	3.4

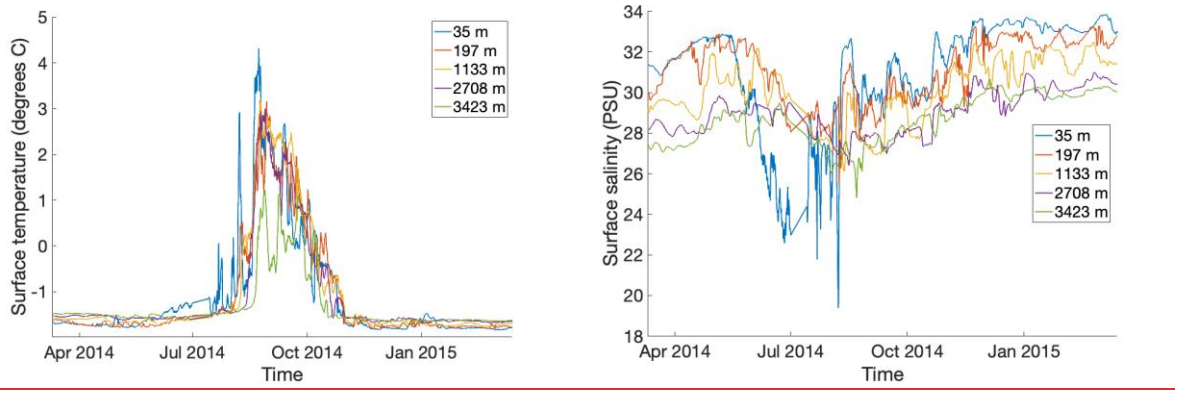

Figure 3. Surface temperature (left) and salinity (right) of the 5 model sites.

4.2 GEM for the Beaufort Sea shelf

Because signal-to-noise ratios appear potentially favorable at the locations that are at least 197 m deep, we constructed a GEM function for the region using "CreateBeaufortGEM.m". To do this, we select all CTD profiles in the region (69–73°N, 160–135°W) from the WOD. This includes a total of 4326 profiles, shown as black dots on Figure 2. We removed suspicious data (e.g. temperature lower than -5°C) and subset to only profiles that extend to at least 50 dbar. This is because the GEM method relies on using a reference pressure which is below the thermocline. The reference pressure was chosen as 50 dbar because many profiles (2981) are retained. Choices of higher reference pressures (deeper depths) lead to much lower numbers of profiles. For example, using 100 dbar as a reference pressure leads to only 2156 profiles. Trial and error with reference pressures of 100 dbar and 150 dbar showed degraded performance relative to 50 dbar. Some CTD profiles from the WOD are near topographic features such as Barrow Canyon. It is possible that this alters the GEM and thus our results. However, eliminating more profiles leads to low fits in the GEM method. This method includes an inherent tradeoff between including CTD profiles from a wider geographic range, which improves the fit of the data, and including data that is from a different dynamical region than the one of interest. Testing a narrower longitude range of CTD profiles yielded similar results to those presented here, suggesting that the method is not too sensitive to the exact choices of which CTD profiles to include. Next, we estimate dynamic travel times from the CTD profiles, generate a GEM, and use the GEM to estimate temperature and salinity profiles from the dynamic travel time from the model. The temperature and salinity GEMs are shown as Figure 4 and 5.

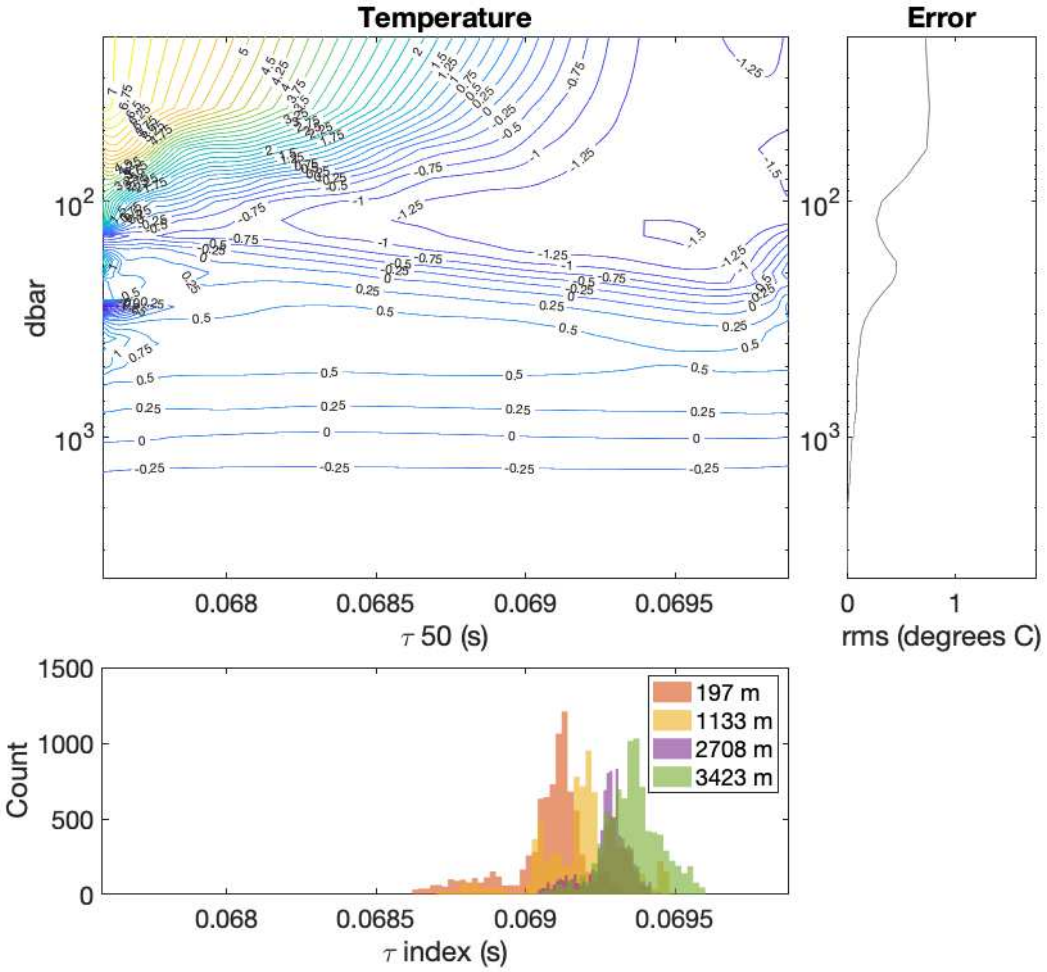

Figure 4. Temperature GEM for Beaufort Sea Shelf.
Upper left plot shows the temperature profile associated with a specific acoustic travel time referenced to 50 dbar, tau_index. Upper right plot shows the root mean square error of the GEM fit to the WOD data as a function of pressure. Lower plot shows a distribution of the values of tau_index at each location taken from one year of ROMS output (no temporal filtering).

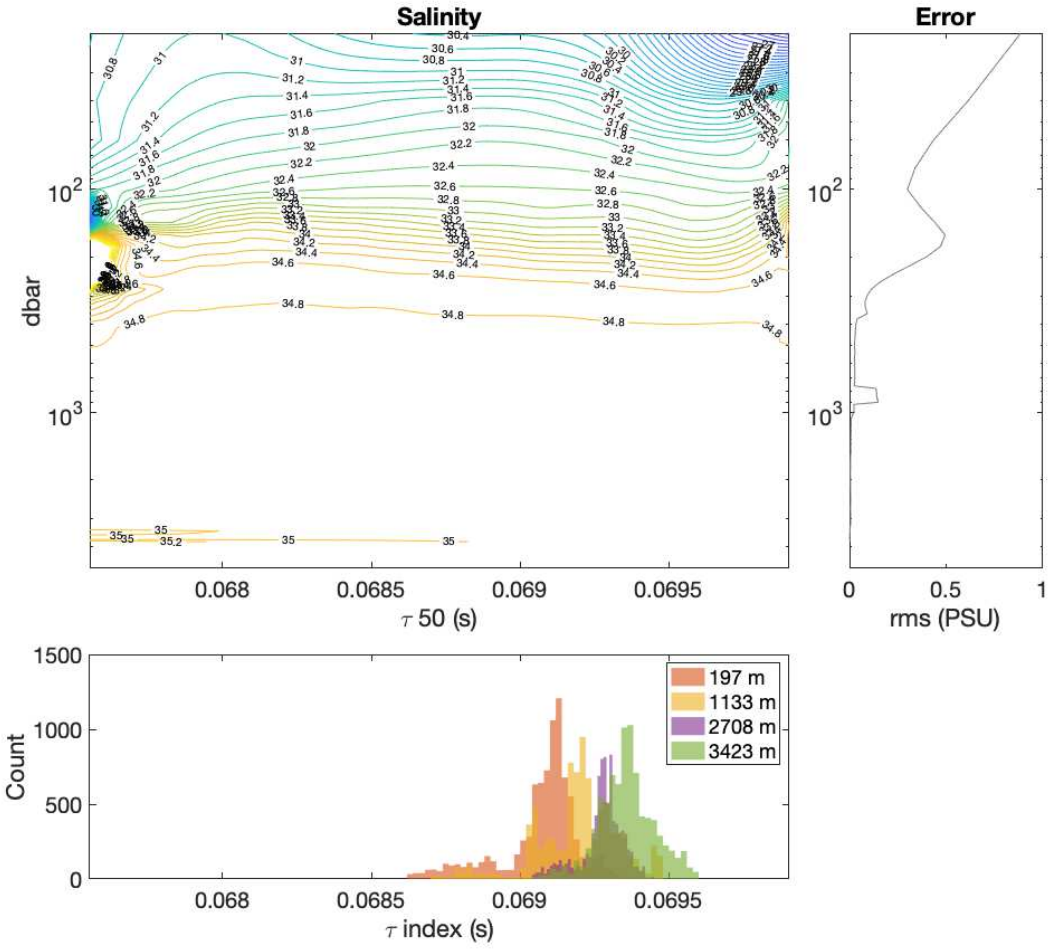

Figure 5. Salinity GEM for Beaufort Shelf.
Upper left plot shows the salinity profile associated with a specific acoustic travel time referenced to 50 dbar, tau_index. Lower plot shows a distribution of the values of tau_index at each location taken from one year of ROMS output (no temporal filtering). Right plot shows the root mean square error of the GEM fit to the WOD data as a function of pressure.

4.3 Estimated errors

Comparing the ROMS temperature and salinity to the GEM estimated temperature and salinity gives an indication of the magnitude of errors anticipated from a CPIES deployed at each location. These are shown in Figures 6–13. Note that this analysis is only conducted for the four locations shown in Figure 2 that extend beyond 50 dbar.

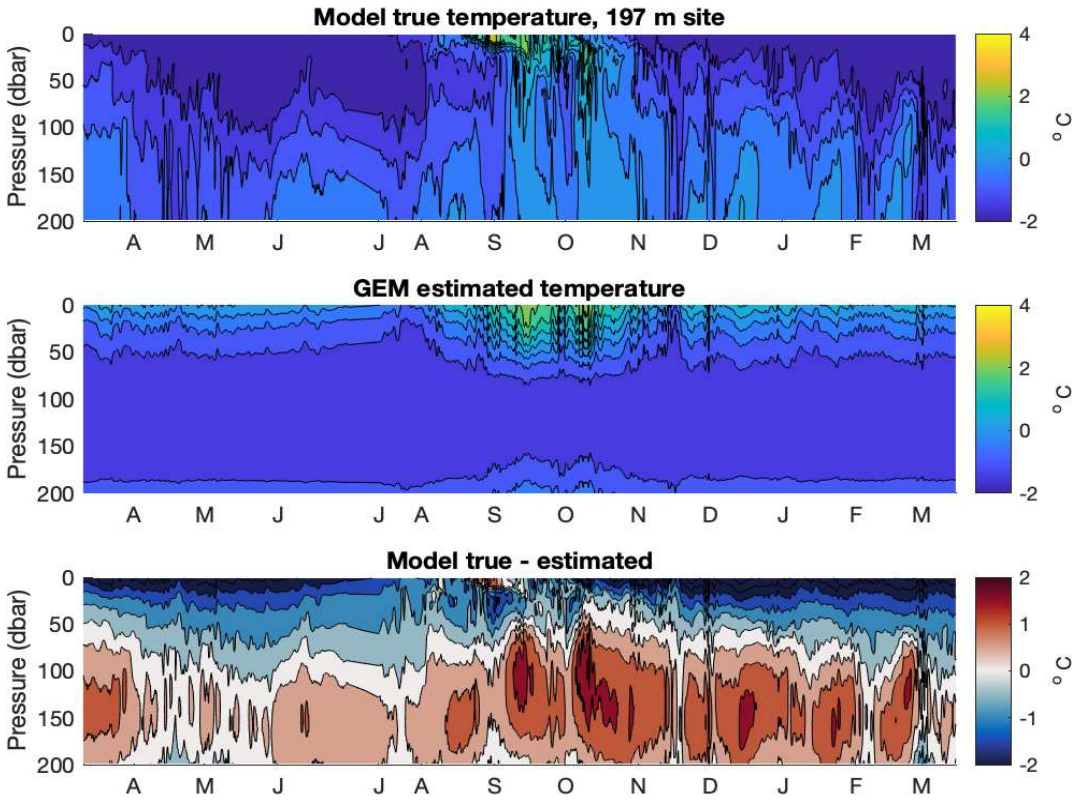

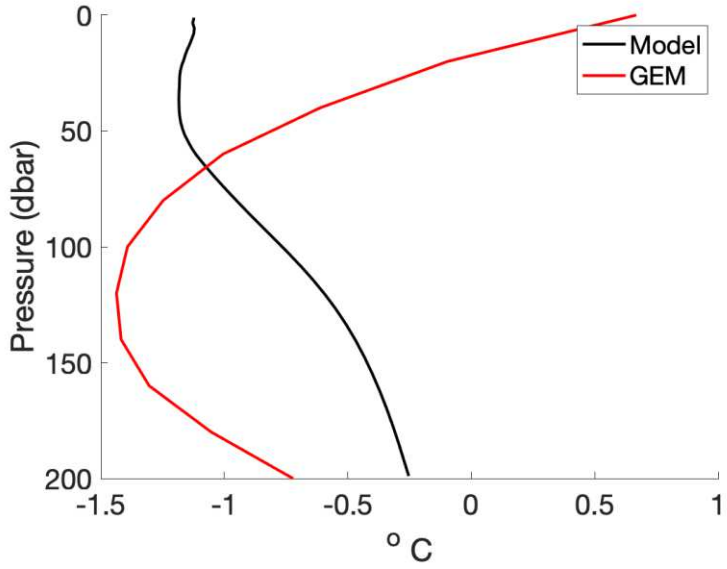

Figure 6. **Top 3 panels**: ROMS temperature, GEM estimated temperature, and difference at 197 m site. Contour intervals are 0.5°C. **Bottom panel**: time mean ROS temperature and GEM estimated temperature.

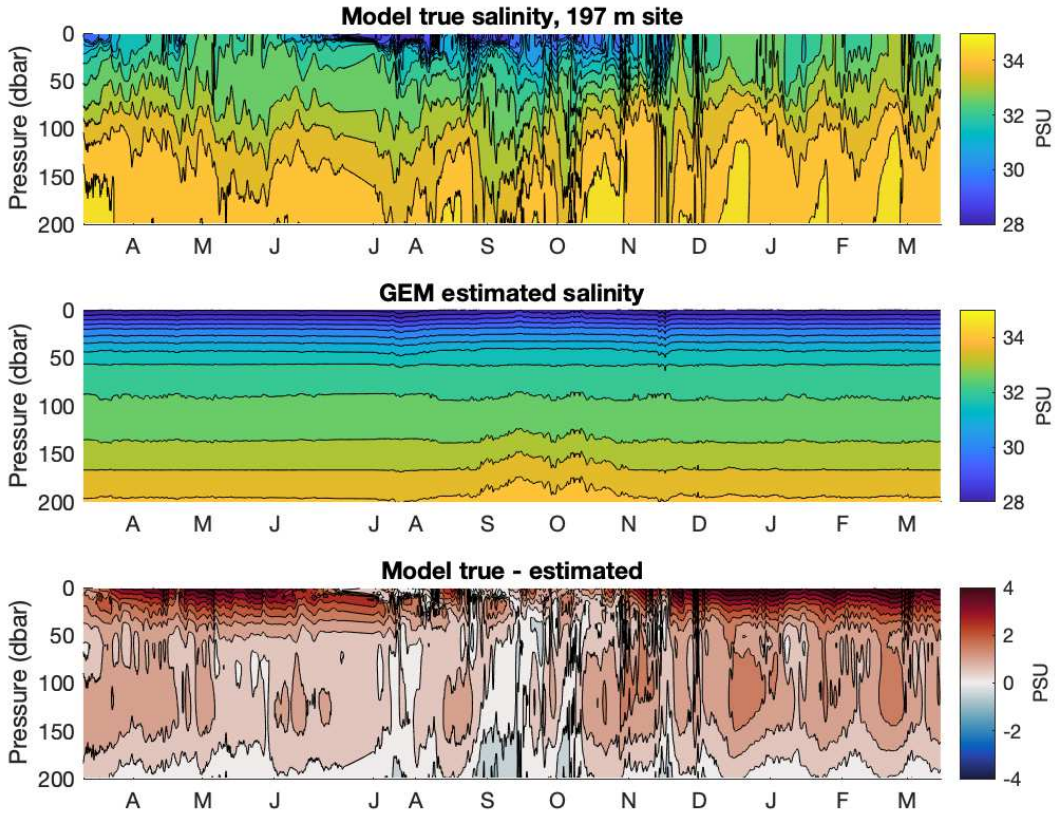

Figure 7. ROMS salinity, GEM estimated salinity, and difference at 197 m site. Contour intervals are 0.5 PSU for top and middle plot, and 0.1 PSU for lower plot.

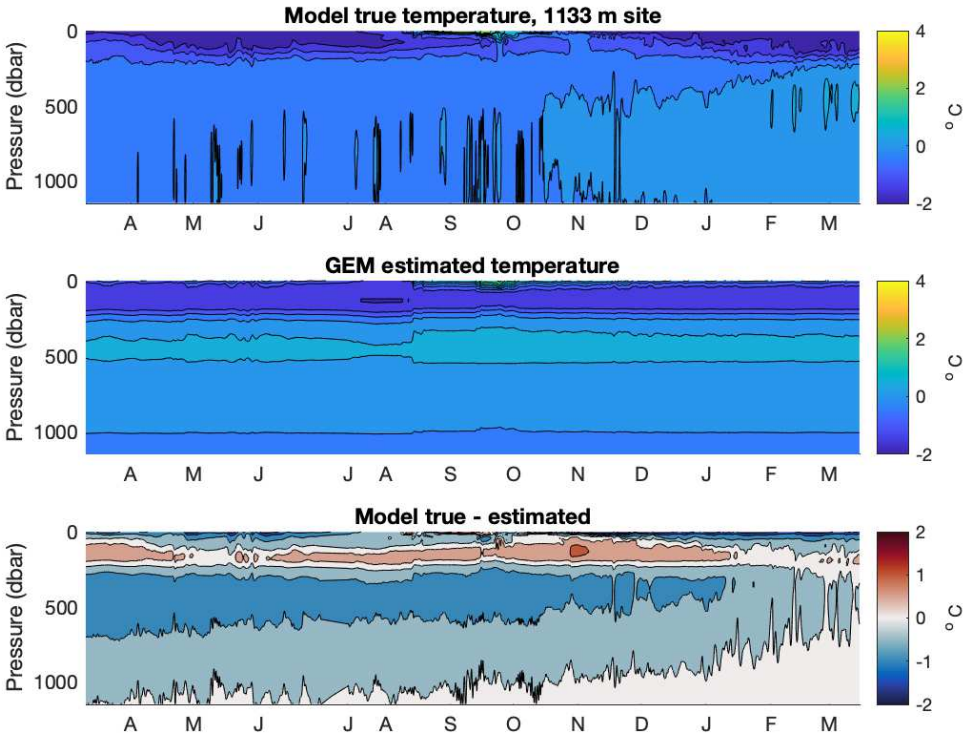

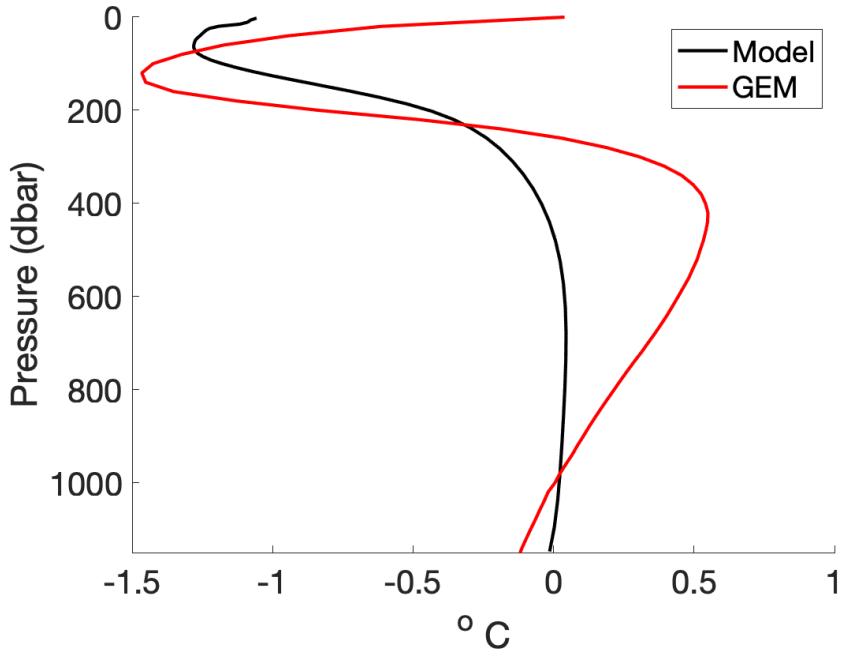

Figure 8. Top 3 panels: ROMS temperature, GEM estimated temperature, and difference at 1133 m site. Contour intervals are 0.5°C. Bottom panel: time mean ROS temperature and GEM estimated temperature.

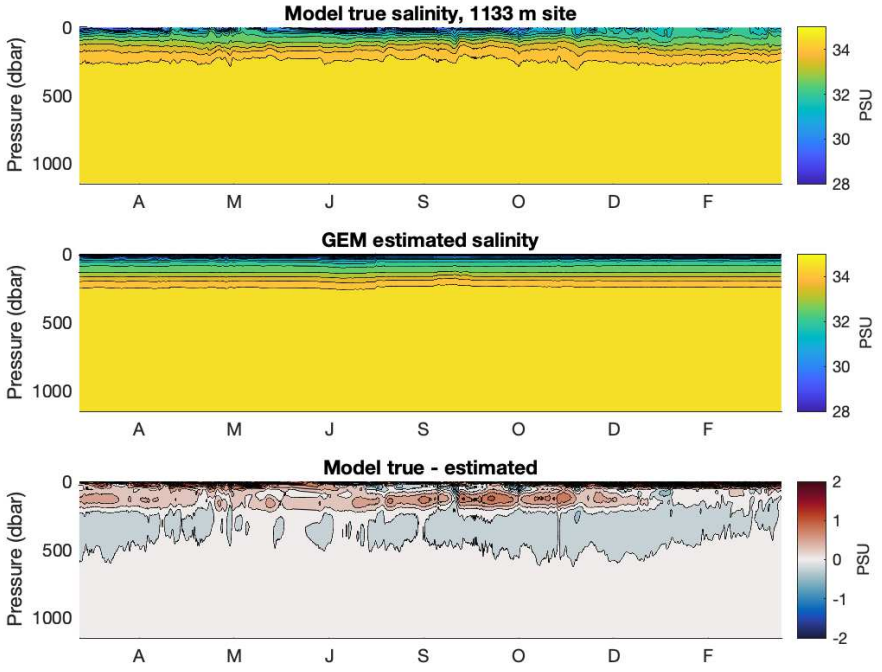

Figure 9. ROMS salinity, GEM estimated salinity, and difference at 1133 m site. Contour intervals are 0.5 PSU for top and middle plot, and 0.1 PSU for lower plot.

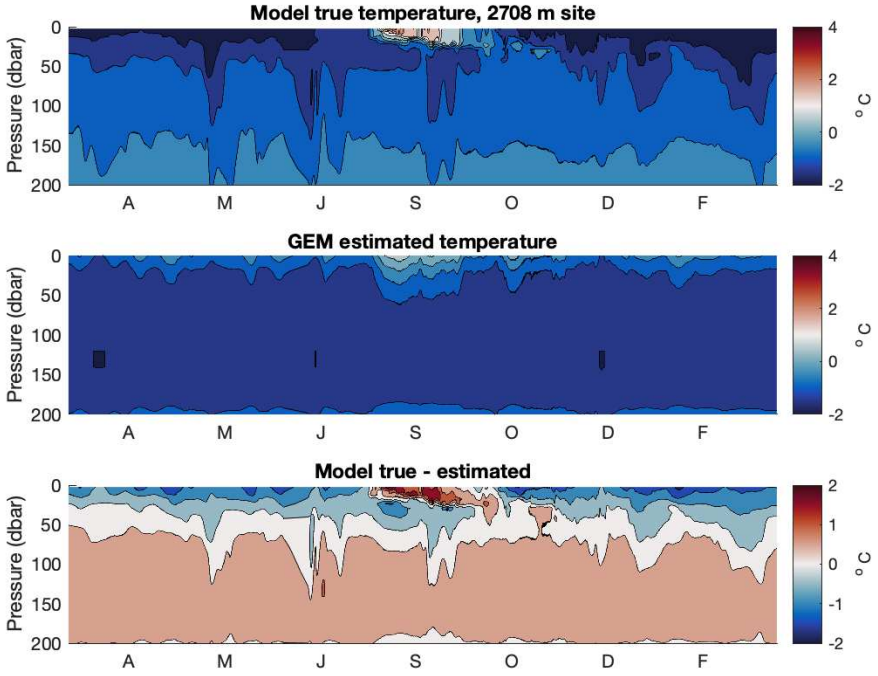

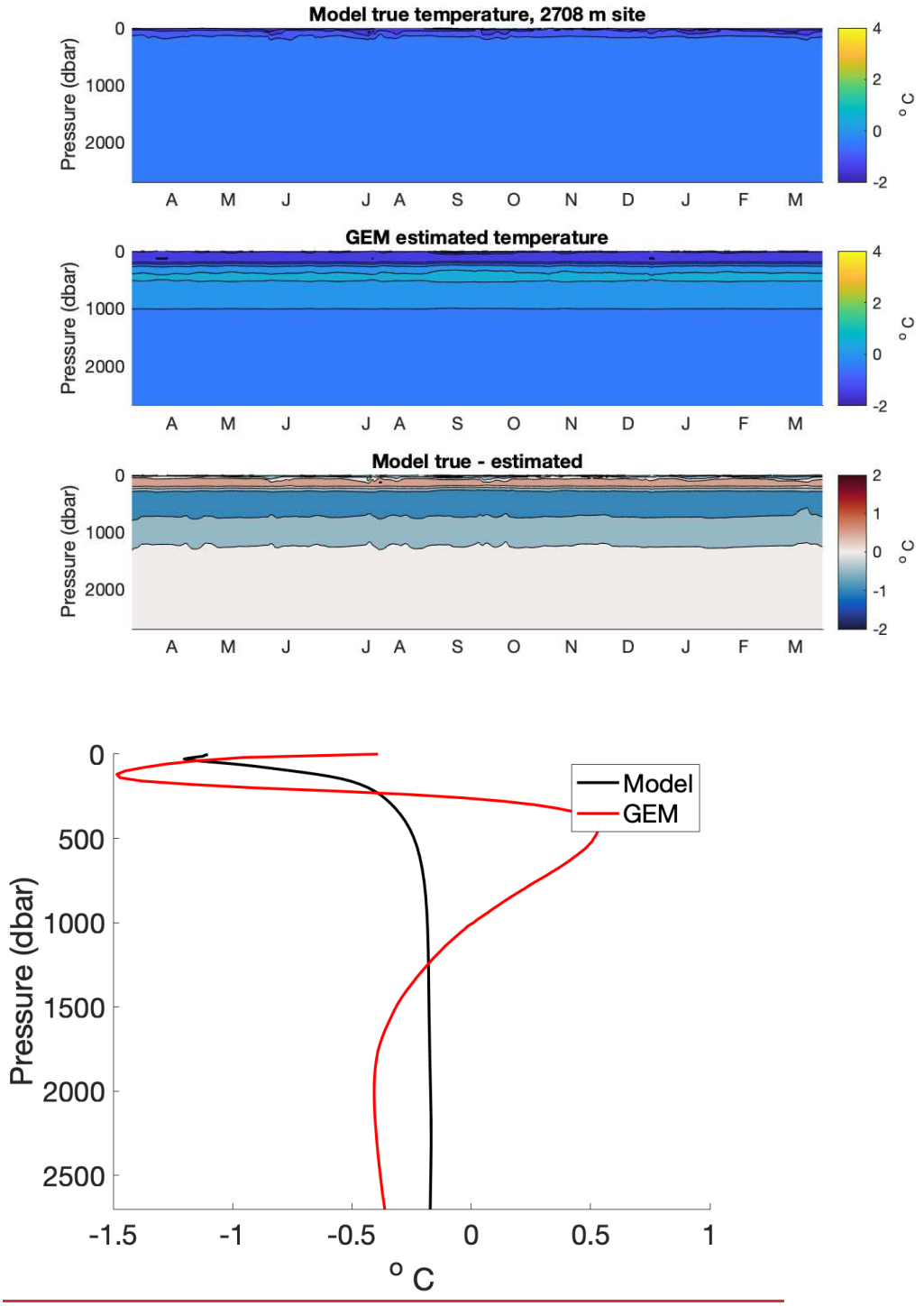

Figure 10. Top 6 panels: ROMS temperature, GEM estimated temperature, and difference at 2708 m site displaying upper 200 m (top 3 plots) and full water column (bottom 3 plots). Contour intervals are 0.5°C. Bottom panel: time mean ROS temperature and GEM estimated temperature.

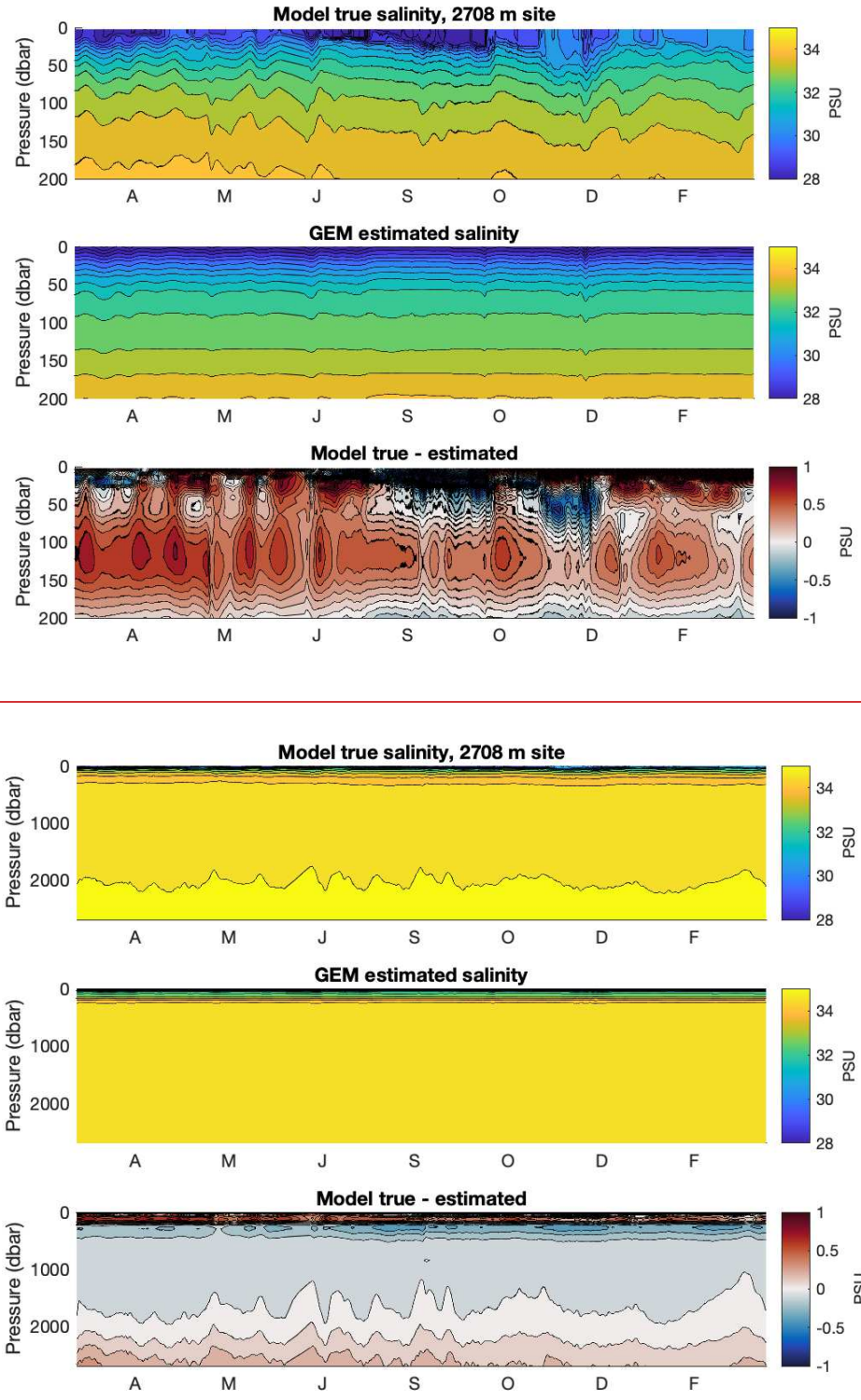

Figure 11. ROMS salinity, GEM estimated salinity, and difference at 2708 m site displaying upper 200 m (top 3 plots) and full water column (bottom 3 plots). Contour intervals are 0.5 PSU for top and middle plot, and 0.1 PSU for lower plot.

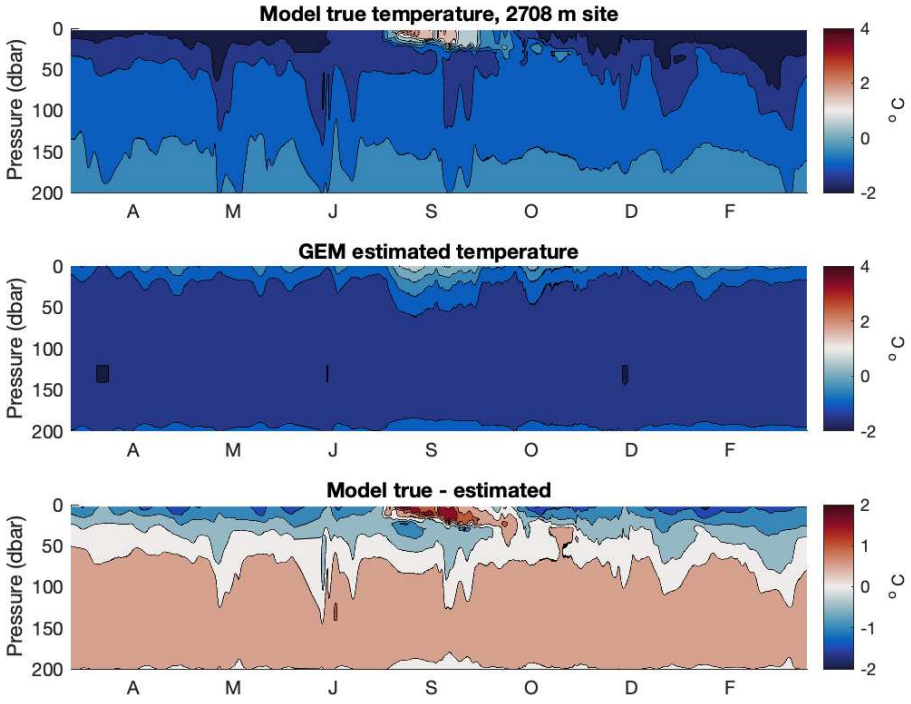
Model true temperature, 2708 m site
Pressure (dbar)
0
50
100
150
200
A
M
J
S
O
D
F
°C
4
2
0
-2
GEM estimated temperature
Pressure (dbar)
0
50
100
150
200
A
M
J
S
O
D
F
°C
4
2
0
-2
Model true - estimated
Pressure (dbar)
0
50
100
150
200
A
M
J
S
O
D
F
°C
2
1
0
-1
-2

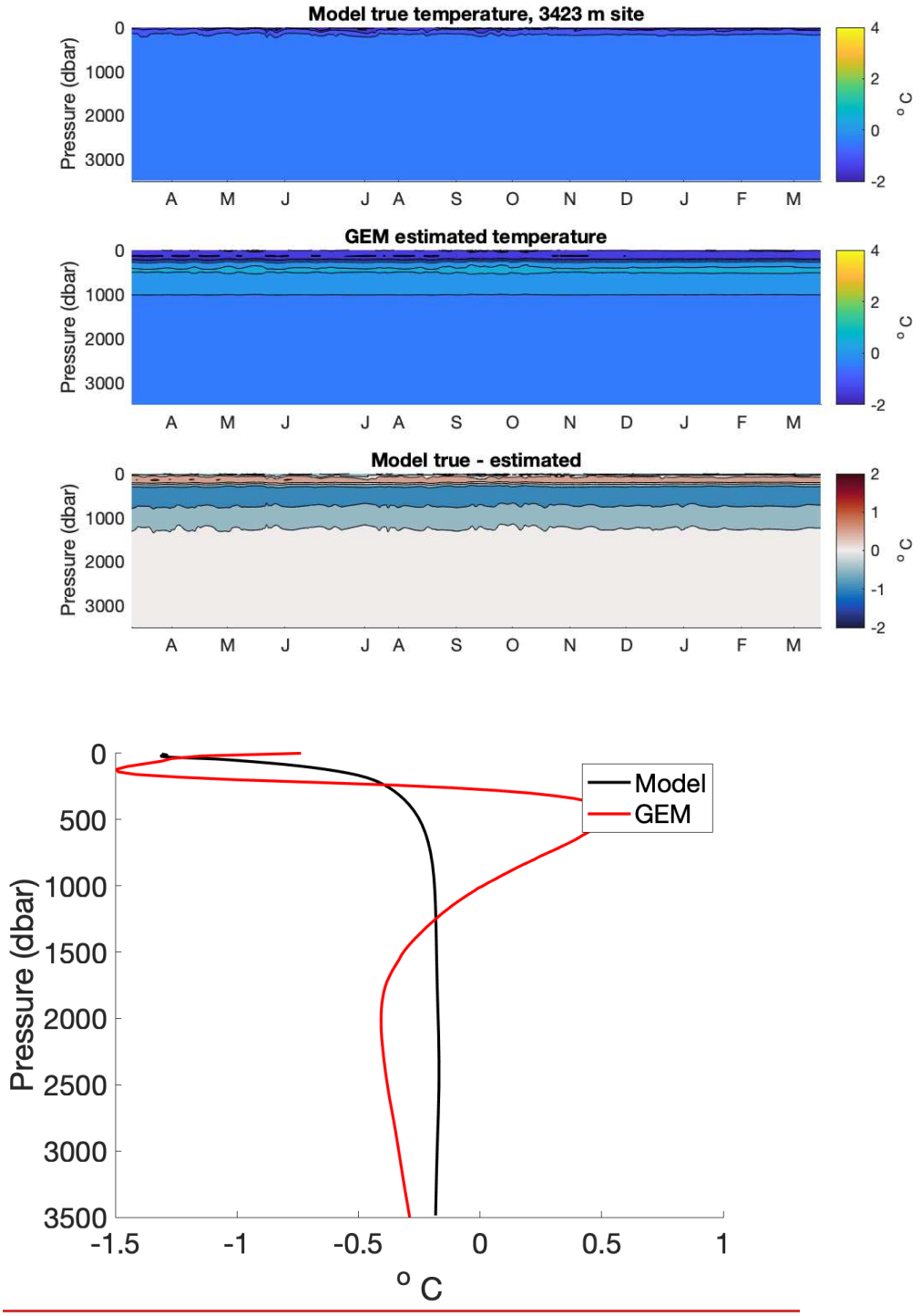

Figure 12. Top 6 panels: ROMS temperature, GEM estimated temperature, and difference at 3423 m site displaying upper 200 m (top 3 plots) and full water column (bottom 3 plots). Contour intervals are 0.5°C. Bottom panel: time mean ROS temperature and GEM estimated temperature.

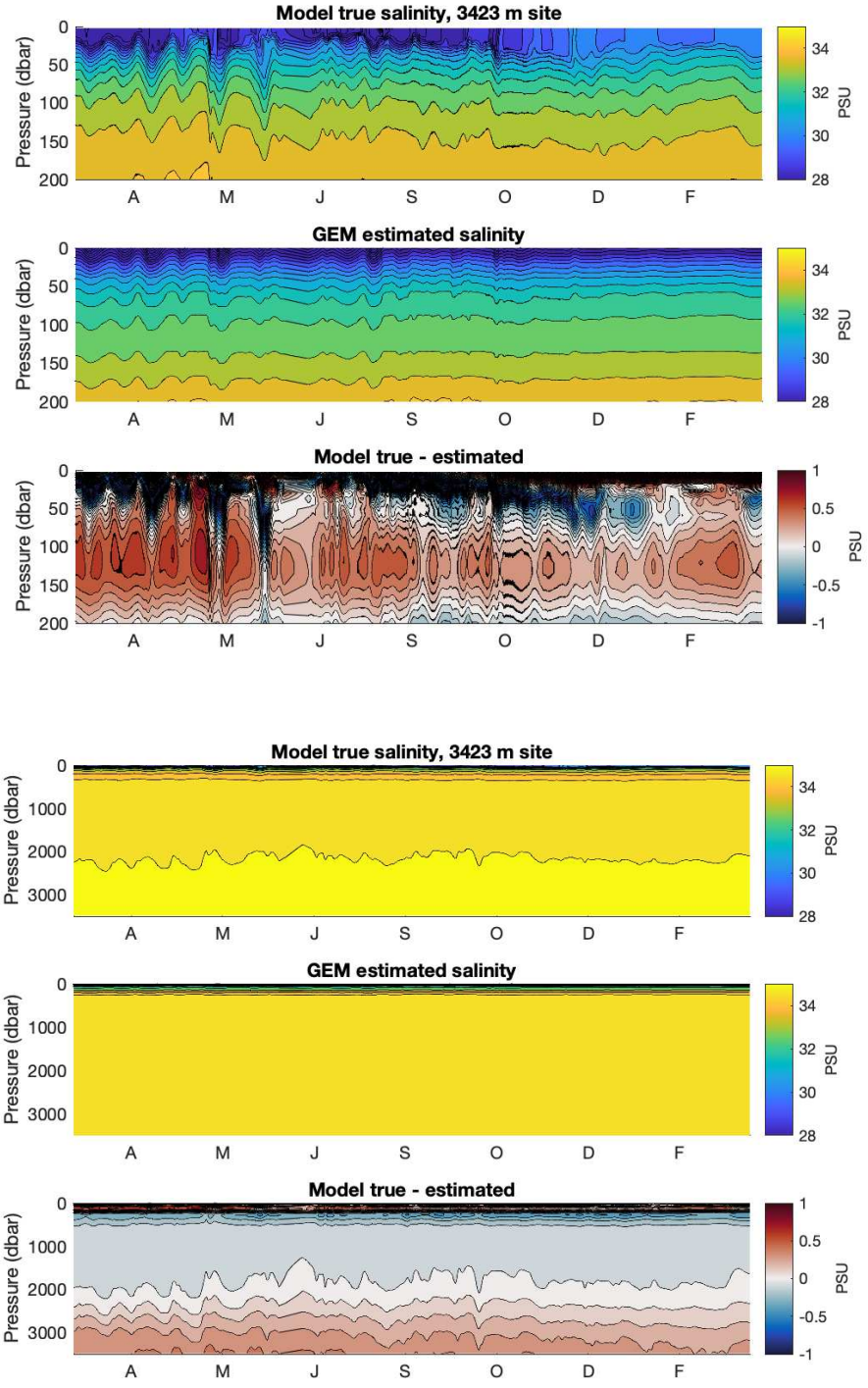

Figure 13. ROMS salinity, GEM estimated salinity, and difference at 3423 m site displaying upper 200 m (top 3 plots) and full water column (bottom 3 plots). Contour intervals are 0.5 PSU for top and middle plot, and 0.1 PSU for lower plot.

In general, errors are on the order of 1–2 °C and 1 PSU. Given the observed range of temperature and salinity, these errors are approximately 17% and 12.5%, respectively. Some of

this error appears to be an offset which is constant in time. For example, based on Figure 6, the GEM method nearly always estimates a temperature which is too warm at the surface and too cold near 125 m depth, compared to the ROMS data. This might emerge from biases between the WOD data used to construct the GEM and the model fields (Figure 14). To assess whether the wide geographic region used for the WOD CTD profiles can explain the difference between observations and the model, we plotted the location of WOD CTD profiles with temperatures warmer than 3°C (Figure 15). These warm locations are widely distributed in space and time, suggesting that the broad region of CTD profiles used is not the reason for mismatches between the model and observations. Thus, the difference may be due to errors in the model, or the inability of the model to resolve the full range of variability in temperature.

The salinity GEM is relatively "flat" over the range of tau_indexes from the model (Figure 5). The temperature GEM is less flat near the surface, but flatter at depth (Figure 4). This means that a change in tau_index corresponds to only a small change in salinity. This makes sense, as the speed of sound has a larger dependence on temperature than on salinity. Thus, errors would be larger.

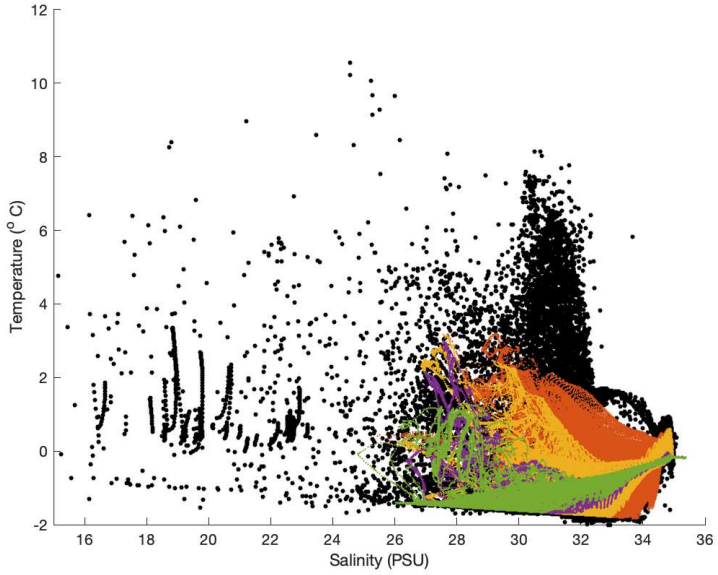

Figure 14. T-S diagram of WOD data (black) and modeled data at each site (colors).

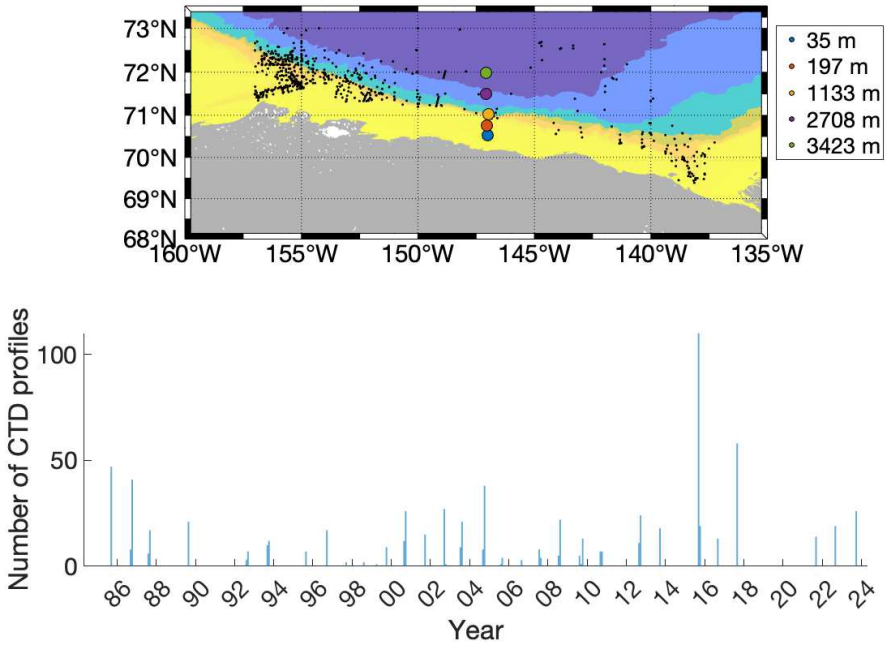

Figure 15. Locations where temperature at any depth was greater than 3°C from WOD CTD casts.

Despite the errors, there are high correlations between ROMS temperatures and the GEM estimated temperature at the 197 m deep site and within the upper 300 dbar of the 1133 m depth site (Figure 16). The r values of these correlations range from 0.3 to 0.9, suggesting that CPIES can resolve 10–80% of the temporal variability in temperature. Correlations are smaller at depth, likely due to mismatches between the thermal structure of the water column from the model and the GEM estimate (cf. bottom panel of Figure 12). For salinity, the highest correlations are for the 1133 m site and the 3423 m site (Figure 17). In general, salinity correlations are lower. This is expected because temperature has a much tighter relationship with sound speed than salinity does. Baroclinic velocity correlations reach a maximum of about 0.4 at 40 dbar. It is unsurprising that the baroclinic velocity correlations are low, because baroclinic velocity is calculated using temperature and salinity. The low correlations in salinity and, to a lesser extent, deep temperatures, is expected to degrade the baroclinic velocity estimates.

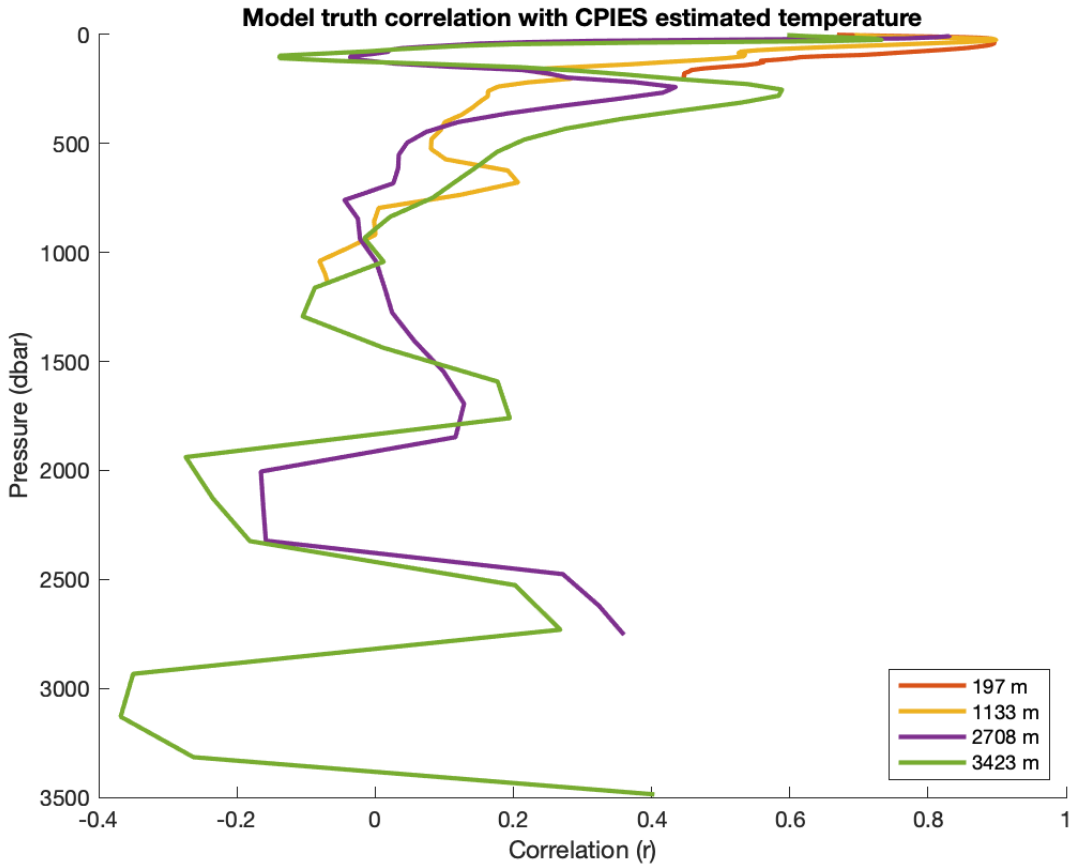

Figure 16. Temporal correlation between ROMS temperature and GEM estimated temperature on Beaufort Shelf.

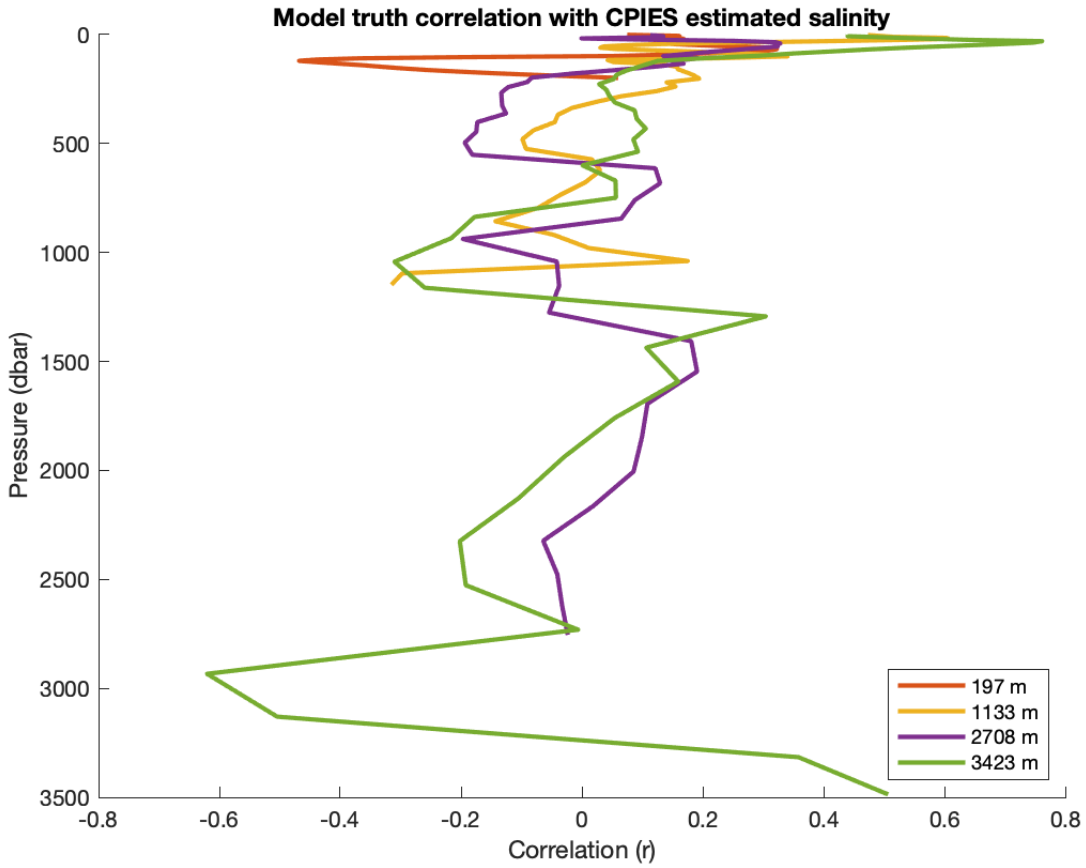

Figure 17. Temporal correlation between ROMS salinity and GEM estimated salinity on Beaufort Shelf.

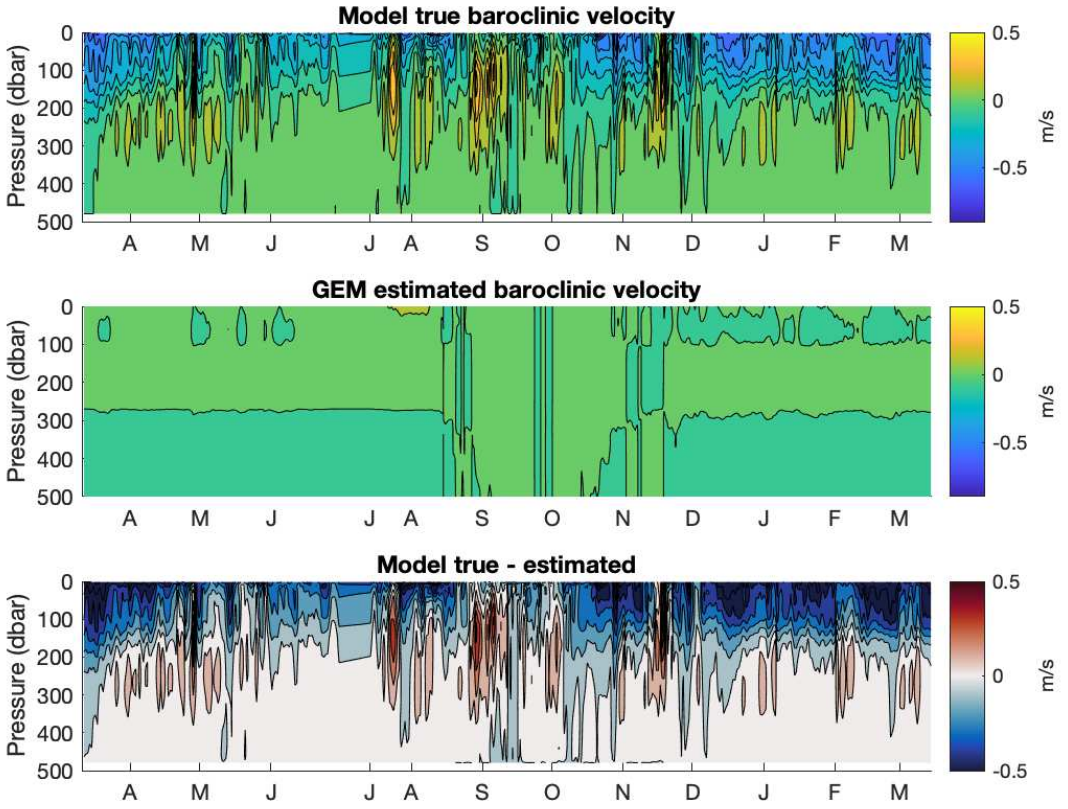

Figure 18. ROMS velocity, GEM estimated velocity, and difference between the two for averaged velocity between 197 and 1133 m sites. Contour intervals are 0.1 m/s.

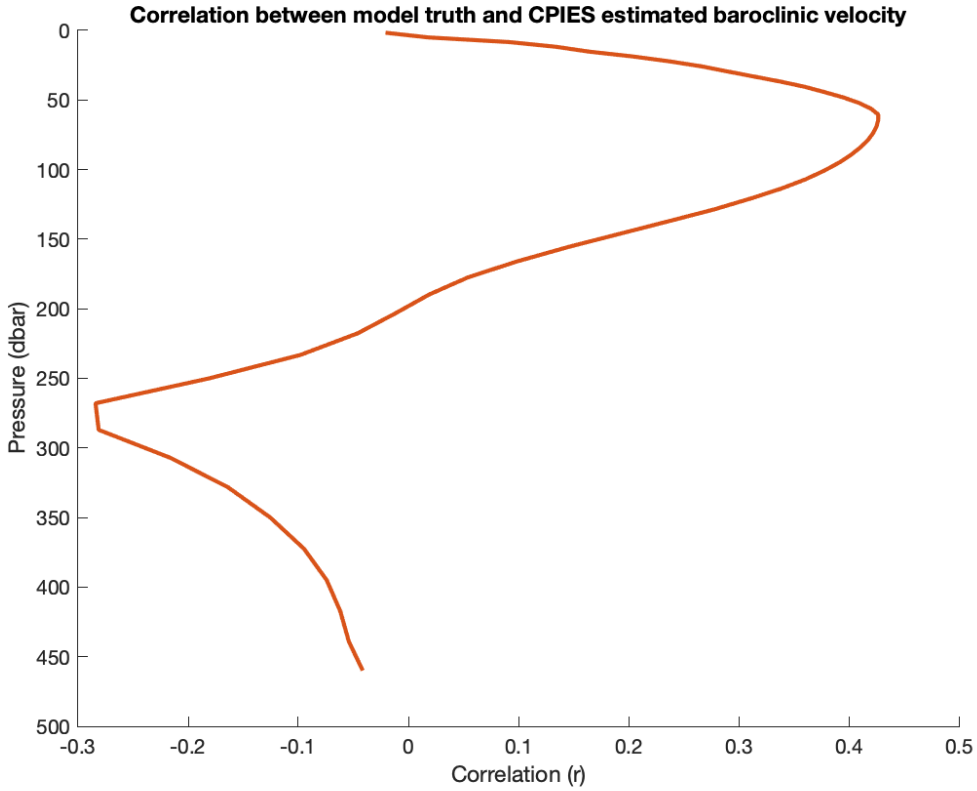

Figure 19. Temporal correlation between ROMS velocity and GEM estimated velocity on Beaufort Shelf.

4.4 Recommendations

Signal-to-noise ratios and correlations between ROMS data and model GEM estimates over the Beaufort Sea slope suggest that CPIES can provide information on temperature and salinity variability. This would provide novel observations, as CPIES can measure the full water profile under sea ice. Moorings deployed under sea ice generally cannot resolve the full T/S profile as ice keels would destroy instruments in the upper part of the water column. However, for CPIES to obtain data with low errors, more in situ observations of temperature and salinity profiles are needed. This could be conducted as part of the same field campaign where CPIES are deployed and recovered. Additional CTD measurements would allow for a more geographically restricted GEM and might lower bias errors seen in Figures 6–13 and 18.

5 Lower Cook Inlet

We assess feasibility at three sites in Lower Cook Inlet, shown in Figure 20. These locations were chosen to cover a range of bottom depths, and to stay relatively closer to where CTD profiles exist. CTD profiles, which are shown as the black dots in Figure 20, come from WOD and the NGA-LTER.

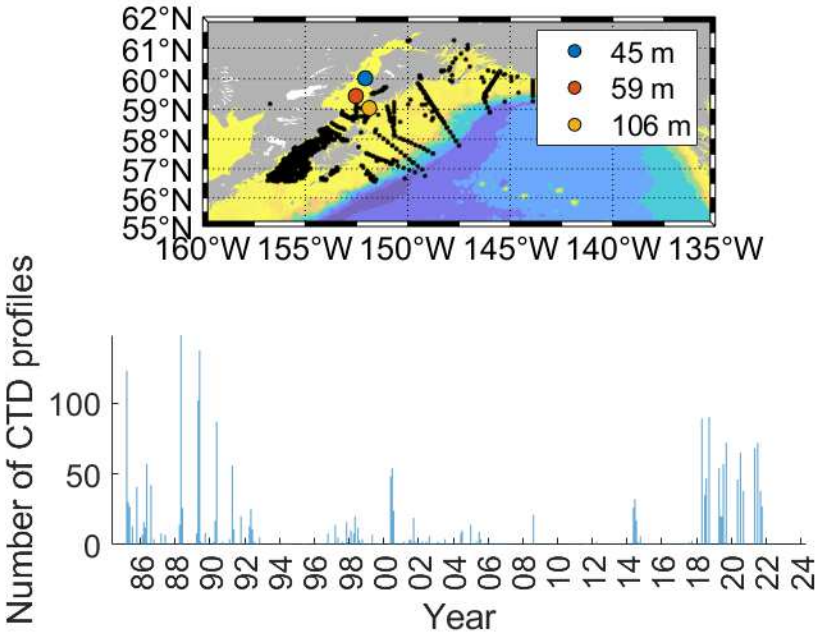

Figure 20. Locations where CPIES feasibility has been assessed in Lower Cook Inlet. Black dots show locations of CTD observations in the region from the World Ocean Database and Northern Gulf of Alaska Long Term Ecological Research. Bottom panel shows distribution of CTD observations in time.

5.1 Signal-to-noise ratios

Signal-to-noise ratios for the Lower Cook Inlet sites are shown in Table 2. All three sites have signal to noise ratios high enough (significantly above 1) to suggest potential feasibility for using CPIES in Lower Cook Inlet.

Table 2. Signal-to-noise ratios in Lower Cook Inlet.

Longitude	Latitude	Depth	Travel time standard deviation (s)	S/N ratio with standard sample rate	S/N ratio with increased sample rate
152.07°W	60°N	**45 m**	4.64×10^{-4}	4.6	7.7
152.5°W	59.43°N	**59 m**	4.78×10^{-4}	4.8	8.0
151.92°W	59.03°N	**106 m**	6.61×10^{-4}	6.6	11.0

5.2 GEM

To construct the Lower Cook Inlet GEM, we selected all CTD profiles in the region (56.5–62°N, 157–142°W) from the World Ocean Database (WOD). We noticed that the Northern Gulf of Alaska Long Term Ecological Research (NGA-LTER) data was not included in the WOD. Therefore, we added NGA-LTER data from 2018-2022 to increase the number of nearby profiles. This includes a total of 9172 profiles, shown as black dots on Figure 20. Then we subset to only profiles that extend to at least 40 dbar. This is because the GEM method reference pressure is below the thermocline. The refence pressure was chosen as 40 dbar because most profiles (3332) are retained. Deeper choices lead to much lower numbers of profiles. The

GEMs for temperature and salinity are shown in Figures 21 and 22. We retained data from all years, even though there are climate change time period trends in the temperature and salinity data in this region (e.g. Danielson et al., 2022), specifically a multidecadal warming trend is seen at all depths and a freshening trend occurs at the surface. There is no objective method to isolate trends from interannual and decadal variability, making it difficult to remove a trend or determine a year to truncate the data. This region consists of a freshening trend of about -0.1 PSU per decade near the surface (Danielson et al., in prep for submission to JGR Oceans) and a warming trend of 0.22 °C per decade between 1970-2021 (Danielson et al. 2022). These trends are about an order of magnitude smaller than the errors we find in the GEM method (e.g. Figures 23–28), therefore we do not believe the trend plays a large role in the feasibility analysis presented here. Next, we estimate dynamic travel times from the CTD profiles, generate a GEM, and use the GEM to estimate temperature and salinity profiles from the dynamic travel time from the model.

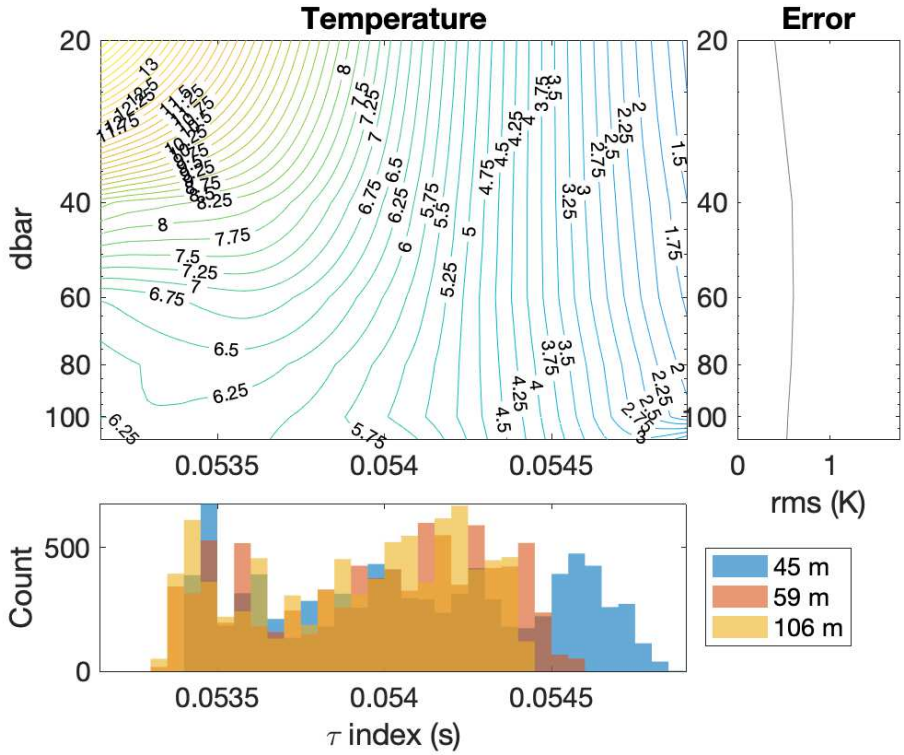

Figure 21. Temperature GEM for Lower Cook Inlet. Upper left plot shows the temperature profile associated with a specific acoustic travel time referenced to 40 dbar, tau_index. Lower plot shows a distribution of the values of tau_index at each location taken from one year of ROMS output (no temporal filtering). Right plot shows the root mean square error of the GEM fit to the WOD data as a function of pressure.

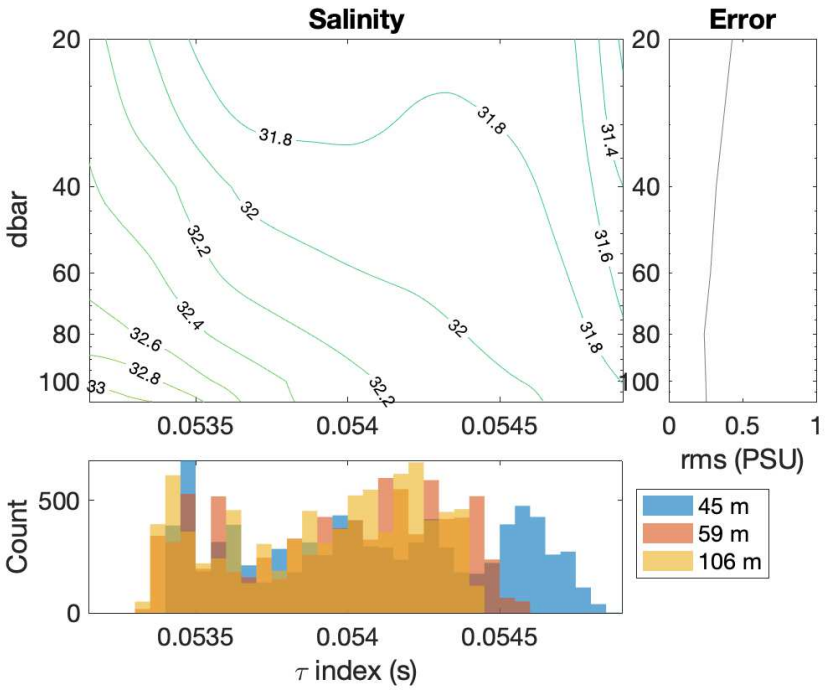

Figure 22. Salinity GEM for Lower Cook Inlet. Upper left plot shows the salinity profile associated with a specific acoustic travel time referenced to 40 dbar, tau_index. Lower plot shows a distribution of the values of tau_index at each location taken from one year of ROMS output (no temporal filtering). Right plot shows the root mean square error of the GEM fit to the WOD data as a function of pressure.

5.3 Estimated errors

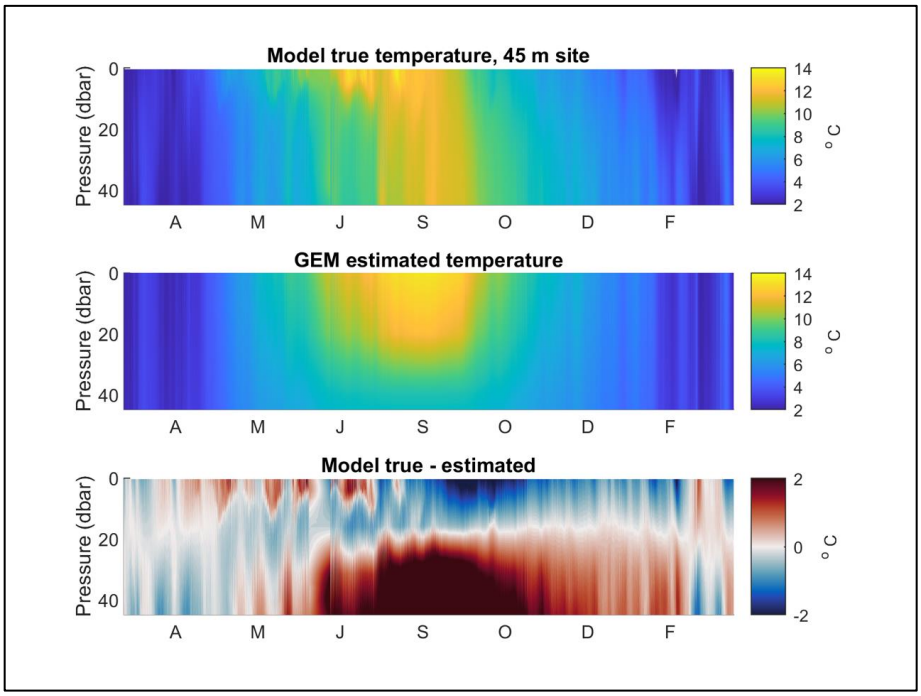

Figure 23. ROMS temperature, GEM estimated temperature, and difference at 45 m site.

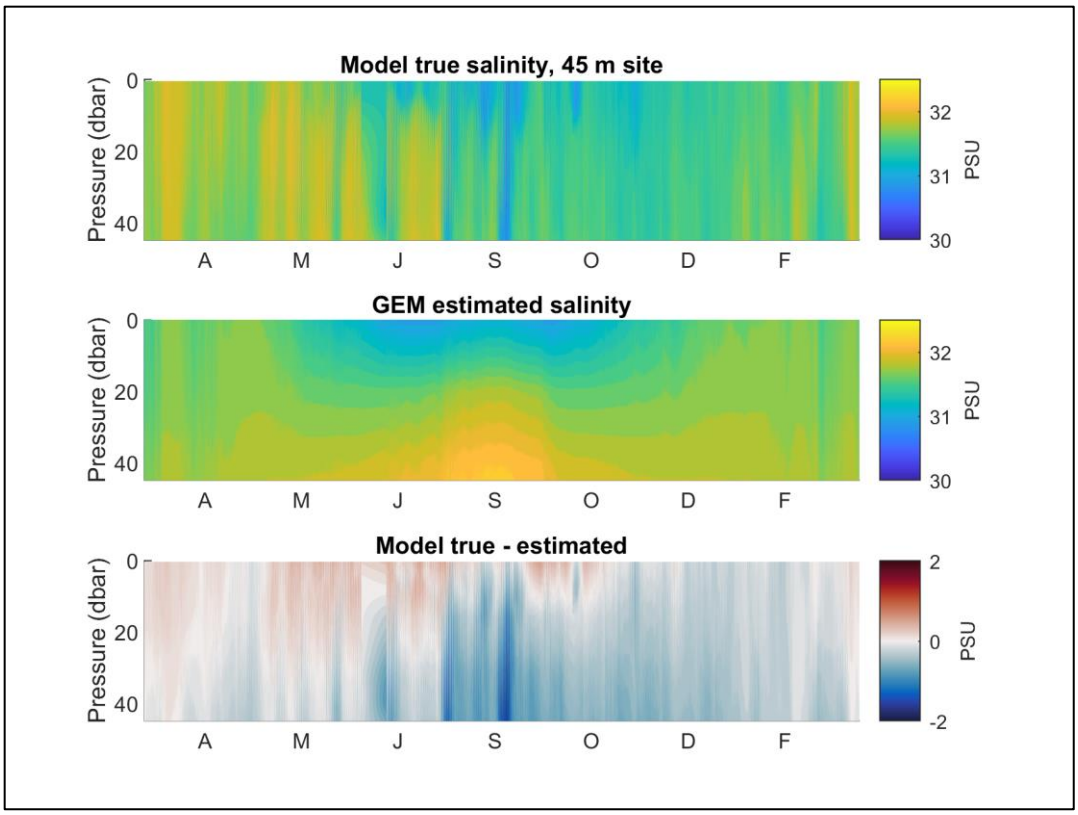

Figure 24. ROMS salinity, GEM estimated salinity, and difference at 45 m site.

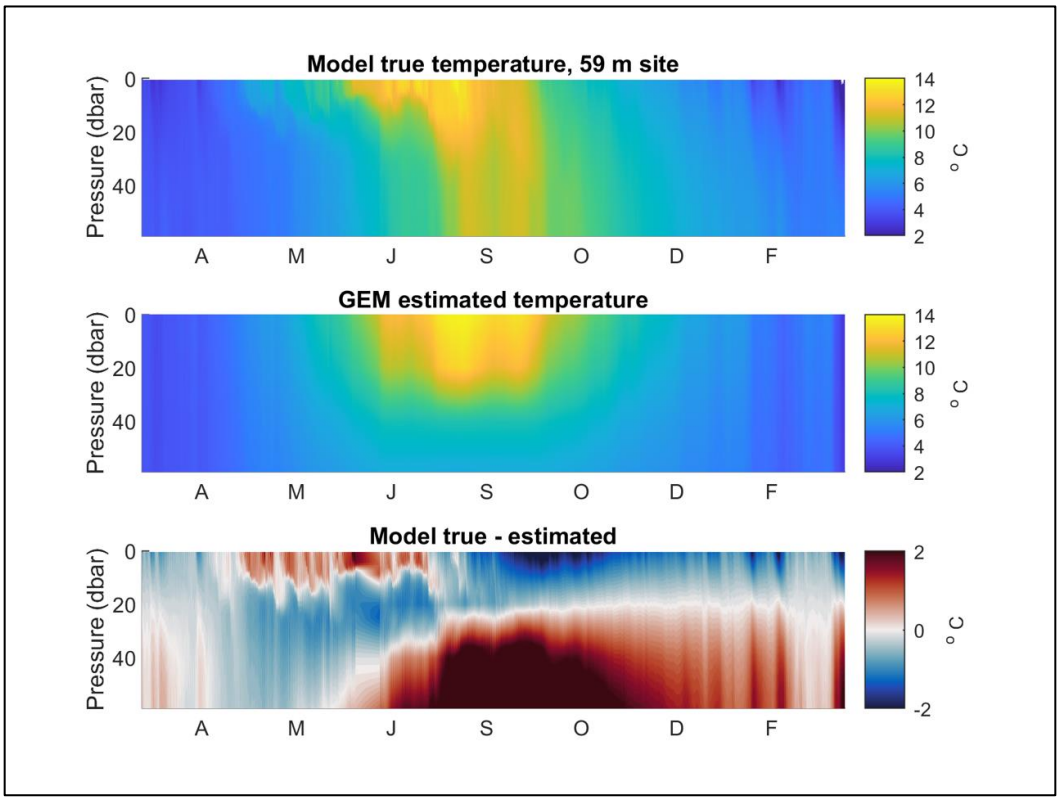

Figure 25. ROMS temperature, GEM estimated temperature, and difference at 59 m site.

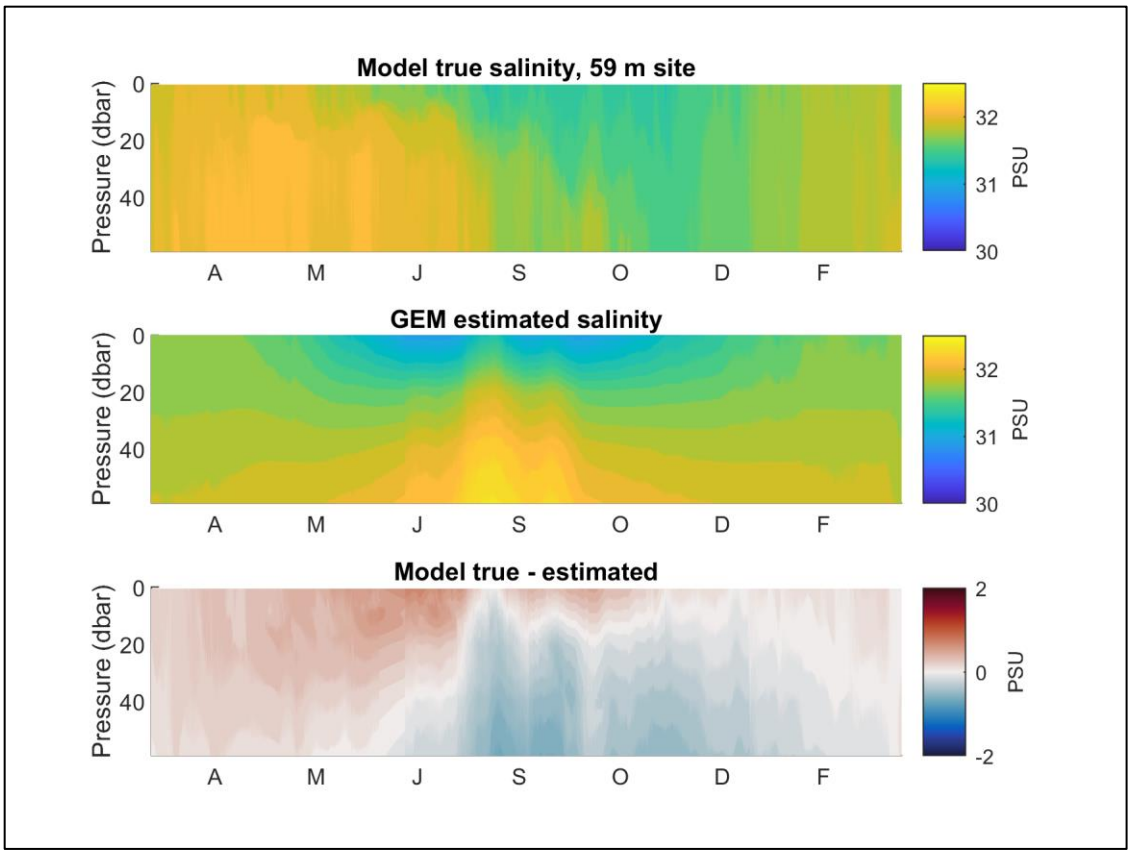

Figure 26. ROMS salinity, GEM estimated salinity, and difference at 59 m site.

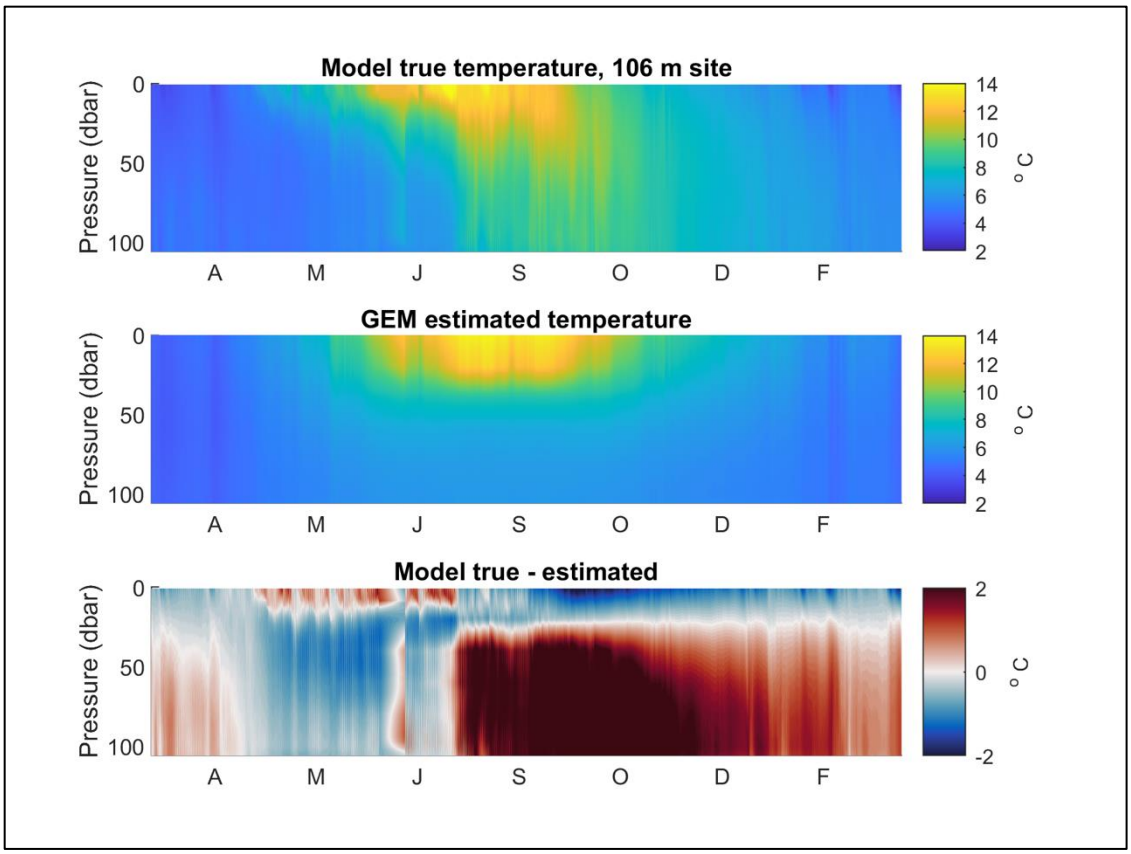

Figure 27. ROMS temperature, GEM estimated temperature, and difference at 106 m site.

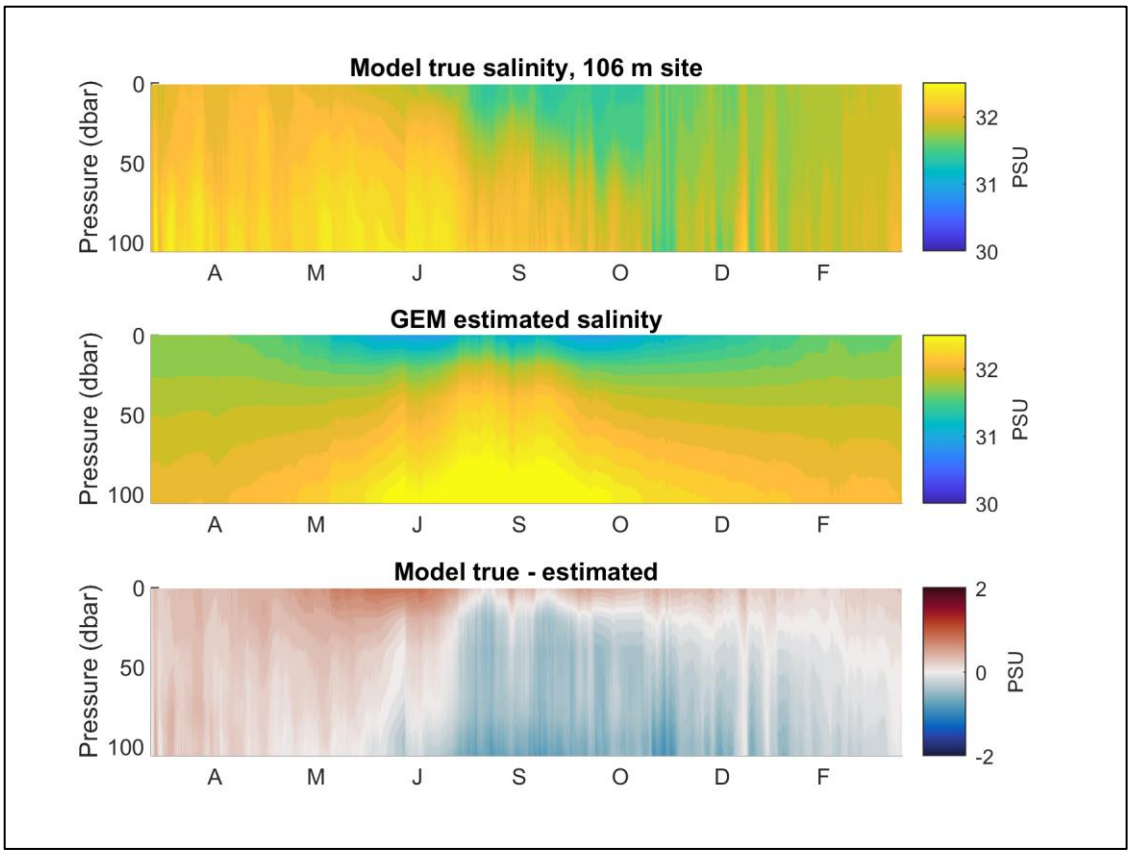

Figure 28. ROMS salinity, GEM estimated salinity, and difference at 106 m site.

The error resulting from comparing the true modeled temperature and salinity to the GEM estimated temperature and salinity are provided as Figures 23-28.

In general, errors are on the order of 1–2 °C and < 1 PSU. Despite the errors, there are high correlations between the model truth temperature and the GEM estimated temperature at all sites at hourly time scales (Figure 29). These correlations are above 0.7, suggesting CPIES can constrain >50% of the temperature variability. The temperature correlation is highest at approximately the depth of the thermocline. This makes sense because the GEM method of mapping acoustic travel time onto a temperature and salinity signal is most adept at tracking the base of the thermocline. Errors are larger both above the thermocline, in the mixed layer, and below the thermocline, as reflected in the r values and in the temperature errors. Salinity correlations are high near the surface but much lower at depth (Figure 30). This is expected because temperature has a much stronger relationship with sound speed than salinity does (e.g. Figure 1). It may also be related to the much wider range of salinities present in the CTD observations compared to the model (Figure 31).

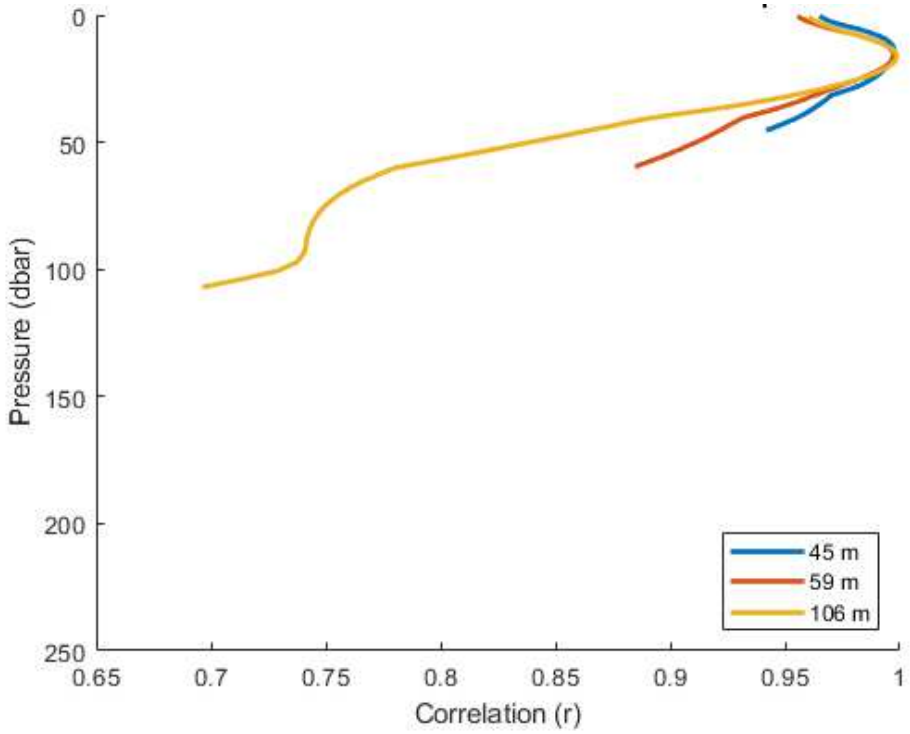

Figure 29. Temporal correlation between ROMS temperature and GEM estimated temperature in Lower Cook Inlet.

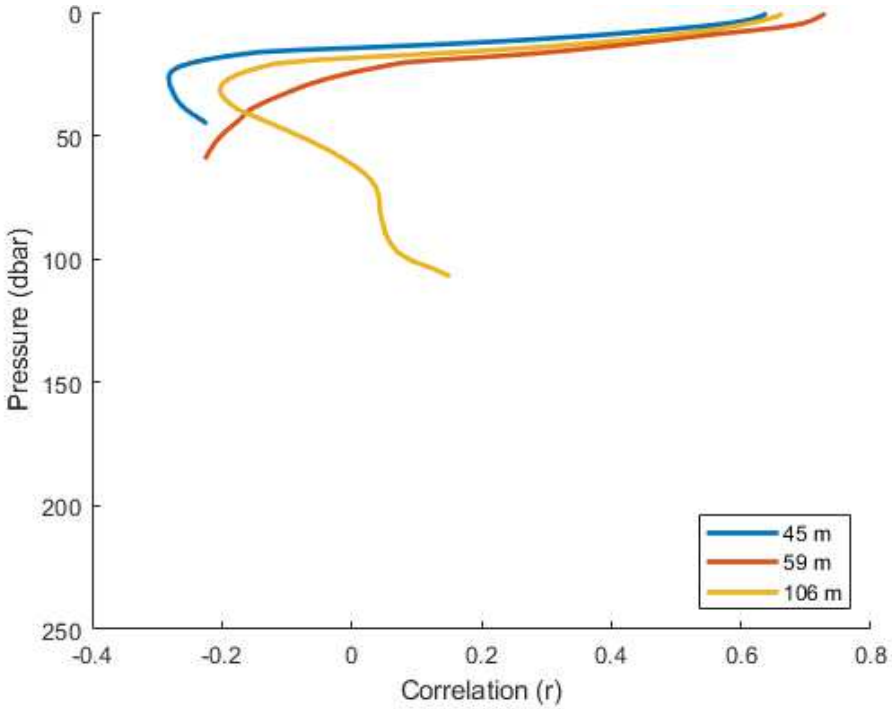

Figure 30. Temporal correlation between ROMS salinity and GEM estimated salinity in Lower Cook Inlet.

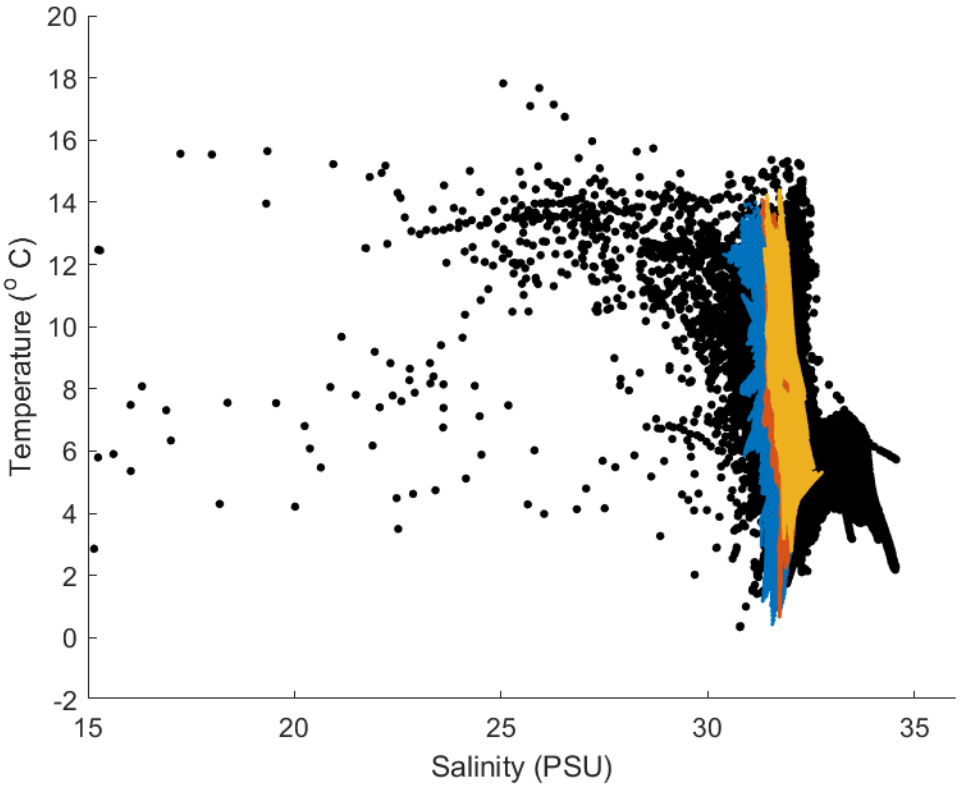

Figure 31. Temperature-salinity diagram from observational data used in the GEM method (black dots) compared to modeled temperature and salinity at the three chosen sites (colored dots).

Because temperature is reasonably simulated at the sites (Figure 28), we investigate whether the velocity between the sites can be simulated using data from the GEM function. Correlations between the model truth and GEM estimated velocities show correlations of r=0.05 to r=0.4 from 10-60 m water depth (Figure 32, 33, 34, 35). This is a low correlation, despite a relatively small bias. We suggest this may be due to the small mean velocity of 0.2 cm/s with low standard deviation of 1.1 cm/s (after 20 hour low pass filtering) between the chosen sites. Errors in salinity also likely play a role. Lastly, in this region, density variability is likely dominated by salinity variability, and salinity has a smaller impact on sound speed than temperature does (Figure 31).

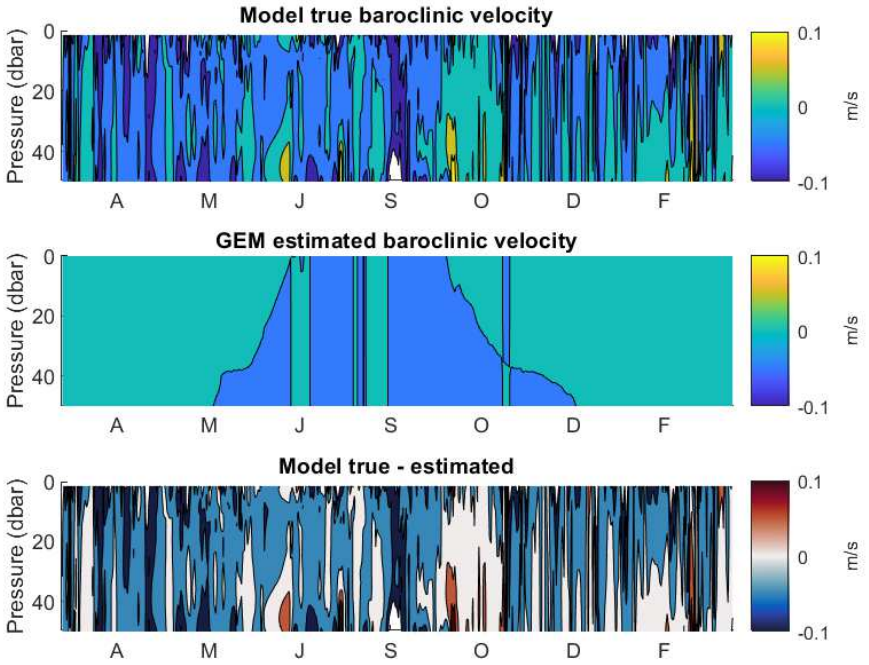

Figure 32. ROMS velocity, GEM estimated velocity, and difference between the two for averaged velocity averaged between the 45 and 59 m sites. Contour intervals are 0.1 m/s.

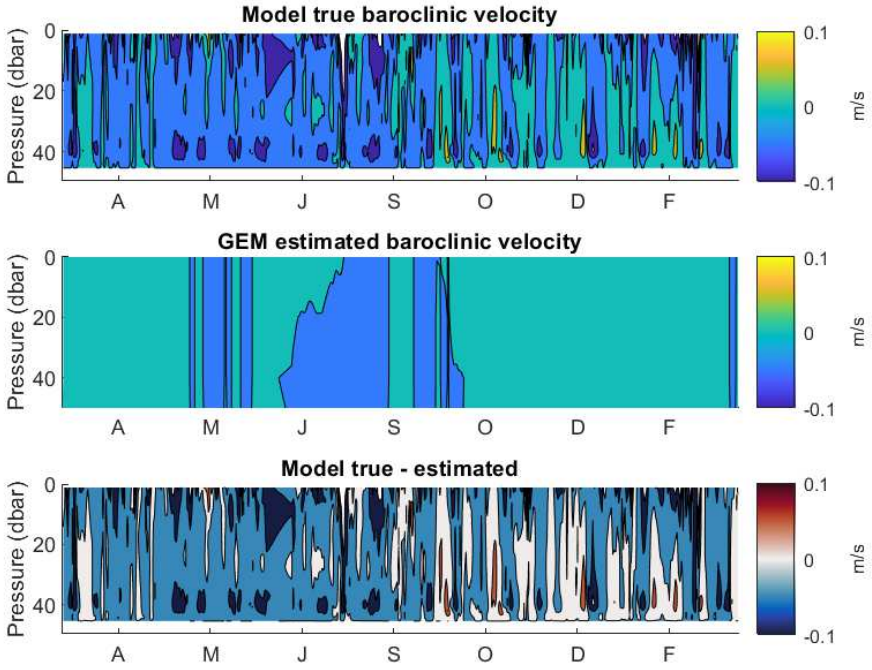

Figure 33. ROMS velocity, GEM estimated velocity, and difference between the two for averaged velocity averaged between the 59 and 106 m sites sites. Contour intervals are 0.1 m/s.

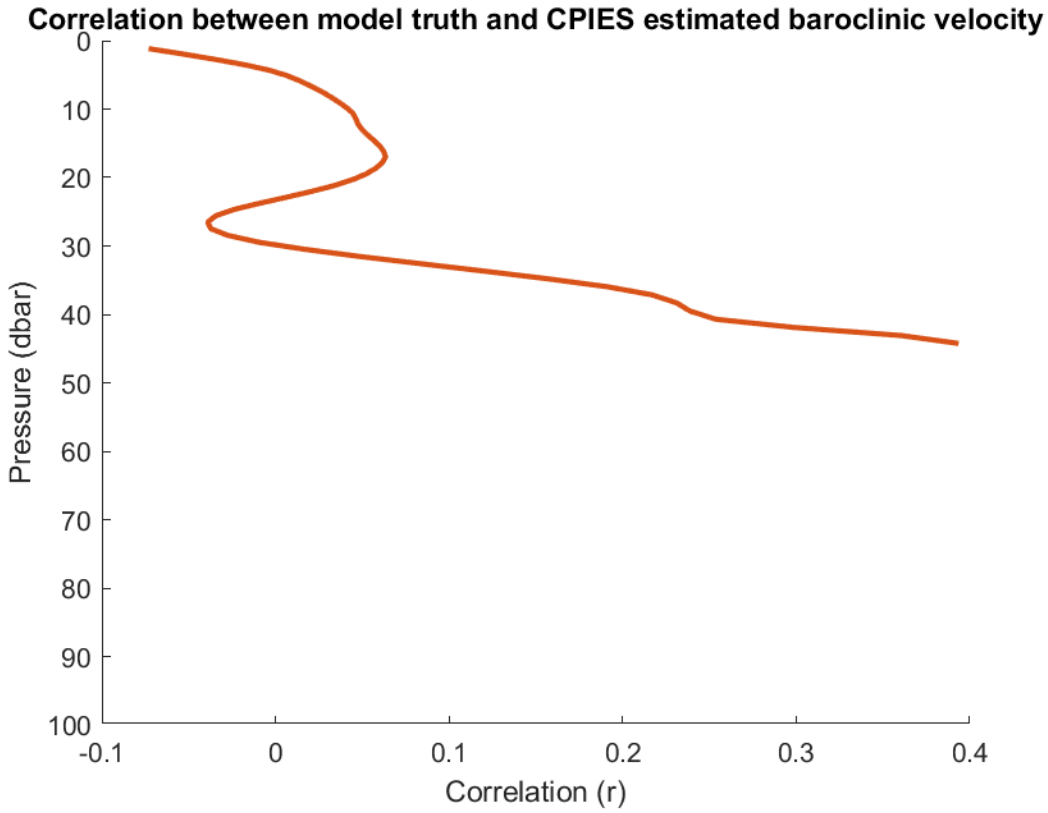

Figure 34. Temporal correlation between model truth baroclinic velocity and GEM estimated baroclinic velocity as a function of depth, between 45 and 59 m sites.

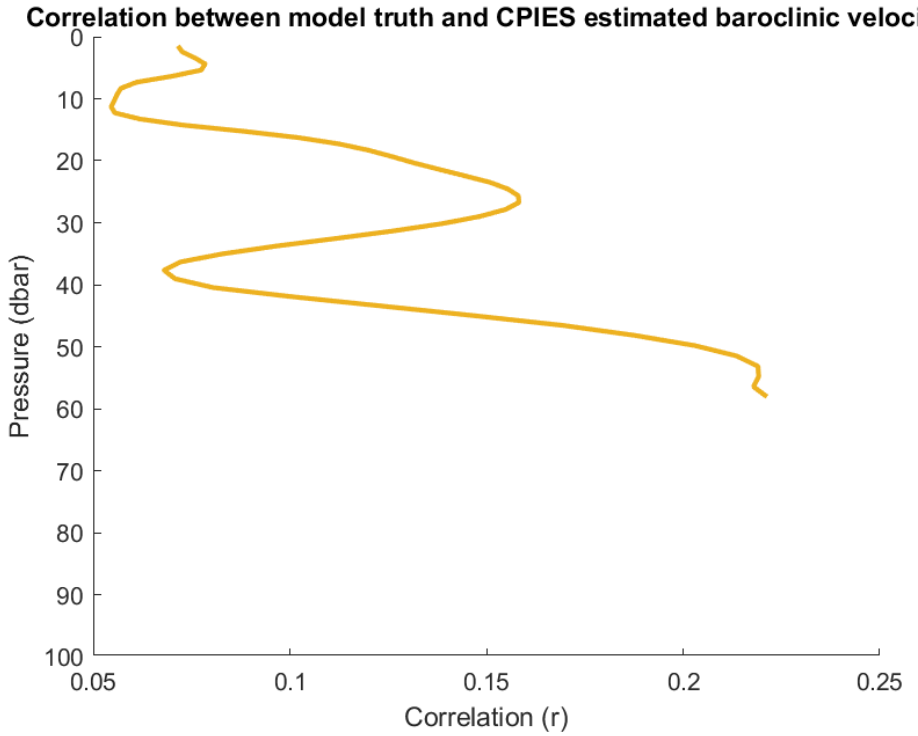

Figure 35. Temporal correlation between model truth baroclinic velocity and GEM estimated baroclinic velocity as a function of depth, between 59 and 106 m sites.

5.4 Recommendations

According to the low pass filtered ROMS output, signal-to-noise ratios are sufficiently large that it is possible to estimate temperature and salinity profiles with the GEM method, at the proposed locations in Lower Cook Inlet. Relatively high hourly correlations in the upper water column temperature data further suggests that the GEM method is appropriate to the proposed three locations. However, correlations between the GEMS method and ROMS model are lower for salinity and geostrophic velocity, even though disagreements (by magnitude of respective units) are smaller than for temperature. It is likely that a component of this is due to the smaller dependence of the speed of sound on salinity than on temperature. A wide range of salinities occur within Lower Cook Inlet (Figure 31), however, the salinity variability will have a relatively small impact on acoustic travel time (Figure 30). Additionally, velocities are small between (in the direction perpendicular to) the chosen sites, which likely reduces the signal and leads to a lower signal to noise ratio.

6 Shelikof Strait

Based on the relatively large (1602) number of CTD profiles in Shelikof Strait in the WOD (Figure 19), we repeat the above analysis for two locations in the lower Strait, near the highest density of CTD profiles. Additionally, we restrict the GEM to only use CTD profiles in or very near to the Strait (Figure 34). We assess two locations, labeled by their depths of 44 m and 221 m.

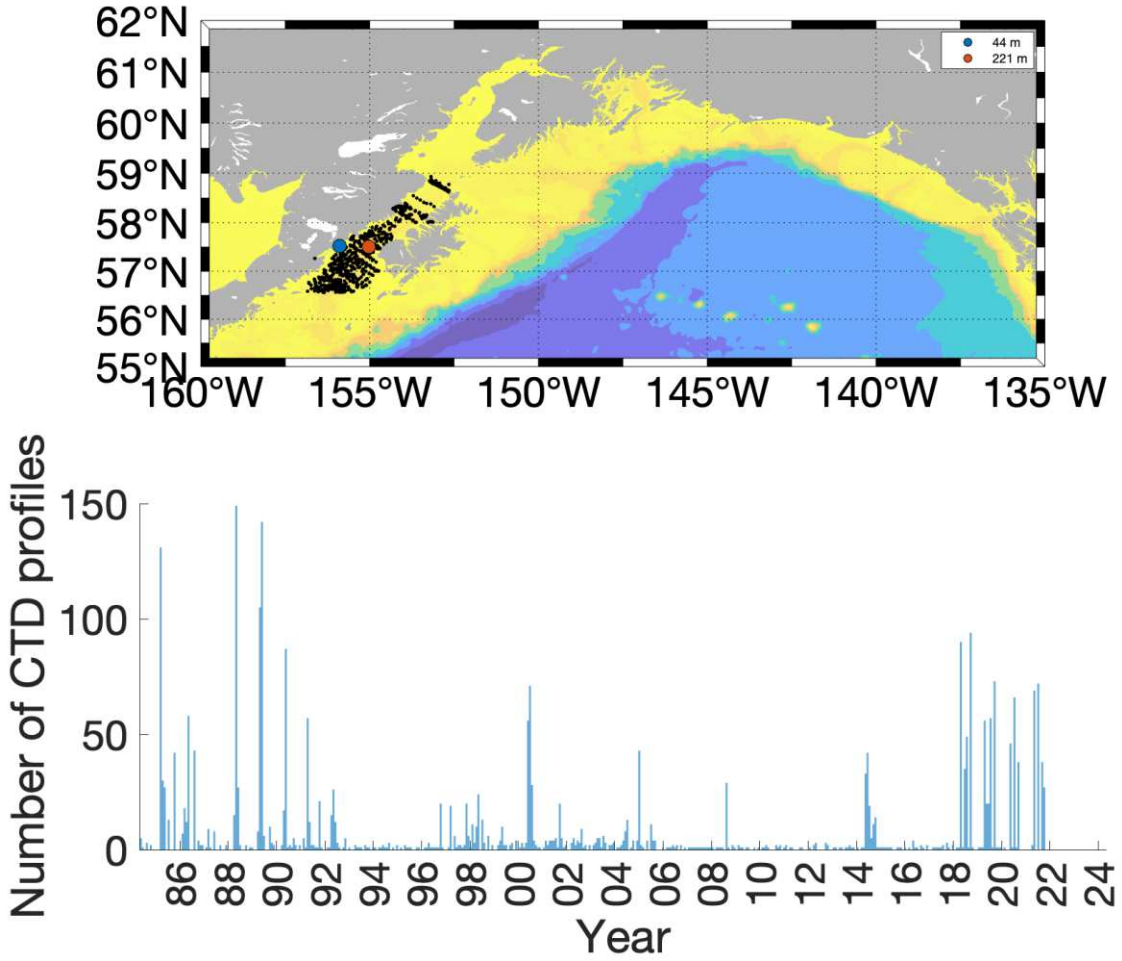

Figure 36. Locations where CPIES feasibility has been assessed within or near Shelikof Strait.

6.1 Signal-to-noise ratios

Signal-to-noise ratios for the Shelikof Strait sites are shown in Table 3. Both sites have signal to noise ratios higher than 6 using the sampling rate from the updated firmware, suggesting potential feasibility for using CPIES in lower Shelikof Strait. The deeper, 221 m site has a signal-to-noise ratio above 10.

Table 3. Signal-to-noise ratios in Shelikof Strait.

Longitude	Latitude	Depth	Travel time standard deviation (s)	Signal-to-noise ratio with standard sample rate	S-to-n ratio with increased sample rate
155.9°W	**57.5°N**	**44 m**	3.86×10^{-4}	3.86	6.43
155°W	**57.5°N**	**221 m**	6.59×10^{-4}	6.59	10.98

6.2 GEM

To construct the Shelikof Strait GEM, we selected all CTD profiles within or near the Strait from the World Ocean Database (WOD). This includes a total of 1602 profiles, shown as black dots on Figure 34. Then we subset to only profiles that extend to at least 40 dbar. This is because the GEM method reference pressure is below the thermocline. The refence pressure was chosen as 40 dbar because most profiles (1474) are retained. The GEMs for temperature and salinity are shown in Figures 35 and 36. Next, we estimate dynamic travel times from the CTD profiles, generate a GEM, and use the GEM to estimate temperature and salinity profiles from the dynamic travel time from the model.

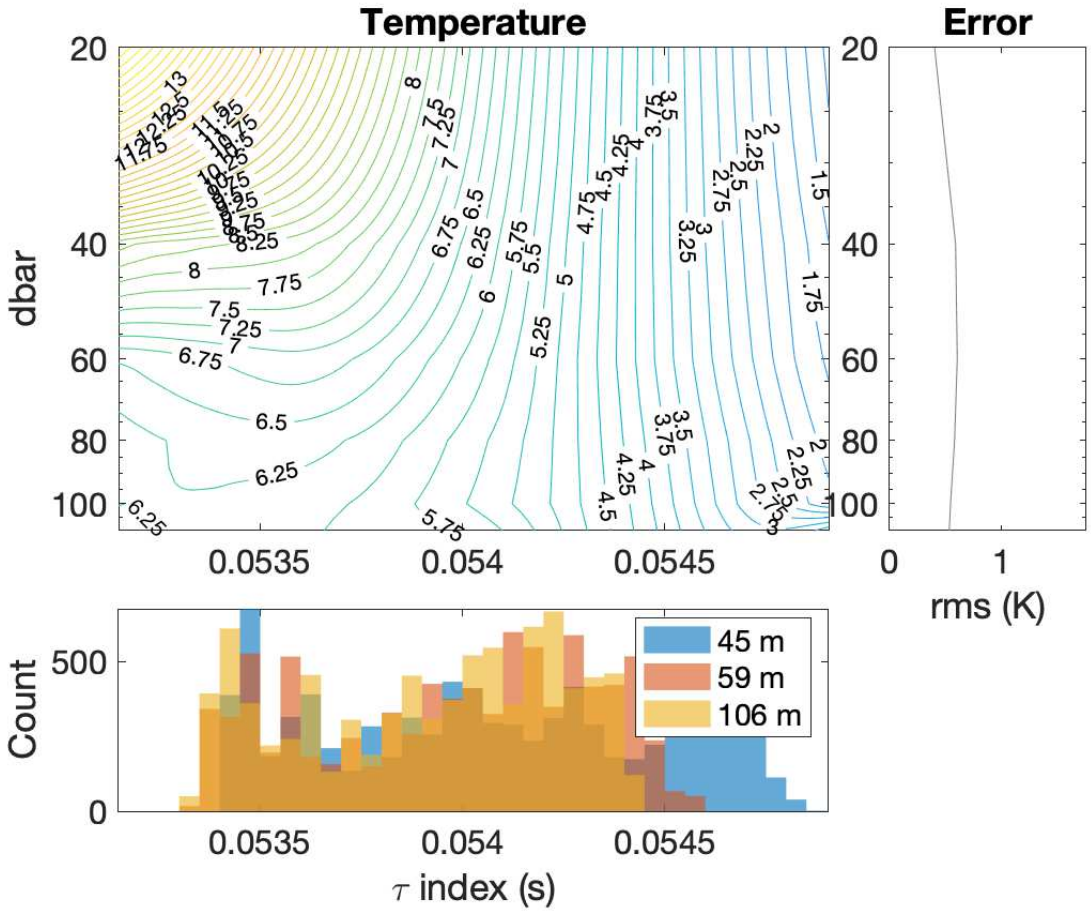

Figure 37. Temperature GEM for Shelikof Strait. Upper left plot shows the temperature profile associated with a specific acoustic travel time referenced to 40 dbar, tau_index. Lower plot shows a distribution of the values of tau_index at each location taken from one year of ROMS output (no temporal filtering). Right plot shows the root mean square error of the GEM fit to the WOD data as a function of pressure. Upper left plot shows the temperature profile associated with a specific acoustic travel time referenced to 40 dbar, tau_index. Lower plot shows a distribution of the values of tau_index at each location taken from one year of ROMS output (no temporal filtering). Right plot shows the root mean square error of the GEM fit to the WOD data as a function of pressure.

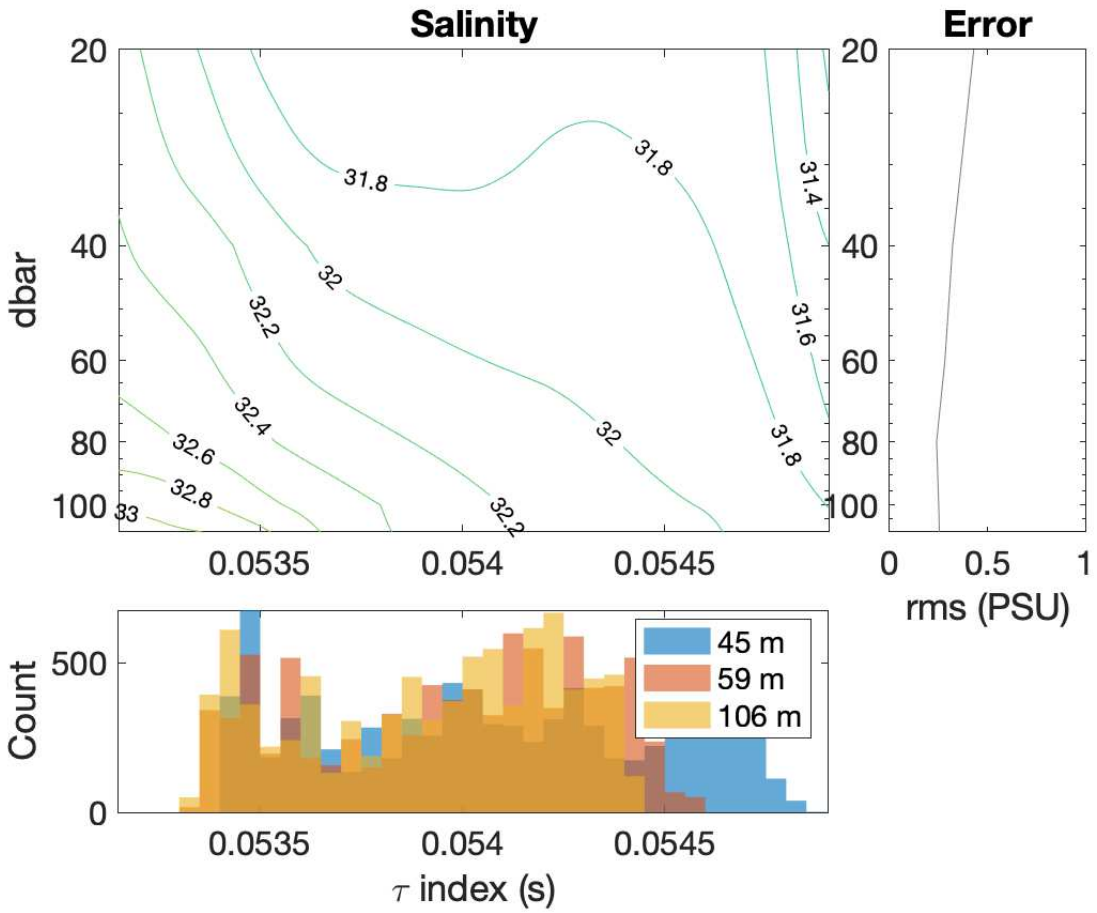

Figure 37. Salinity GEM for Shelikof Strait. Upper left plot shows the temperature profile associated with a specific acoustic travel time referenced to 40 dbar, tau_index. Lower plot shows a distribution of the values of tau_index at each location taken from one year of ROMS output (no temporal filtering). Right plot shows the root mean square error of the GEM fit to the WOD data as a function of pressure.

6.3 Estimated errors

Temperature in Shelikof Strait is well estimated by the GEM (Figure 37, 39), with correlations above 0.8 in the upper 50 m (Figure 41). Salinity correlations are lower than temperature, but higher than in that those estimated in Lower Cook Inlet, with correlations generally higher than 0.3 in the upper 50 m (Figure 42). Baroclinic velocity estimates have lower correlations (Figure 44), perhaps due to errors in the salinity estimates. The GEM estimate is able to resolve some variability in ROMS model velocity, with a peak correlation of about 0.25. Overall, use of CPIES in Shelikof Strait is more promising than in Lower Cook Inlet.

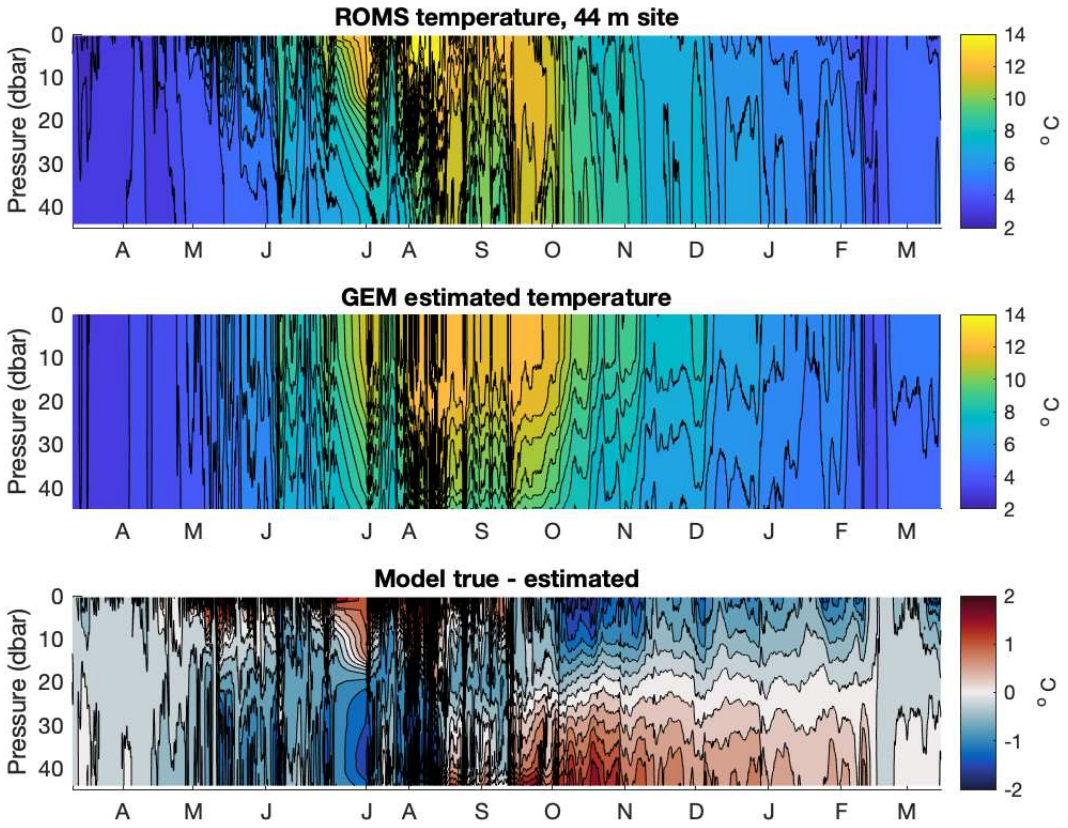

Figure 38. ROMS temperature, GEM estimated temperature, and difference at 44 m site.

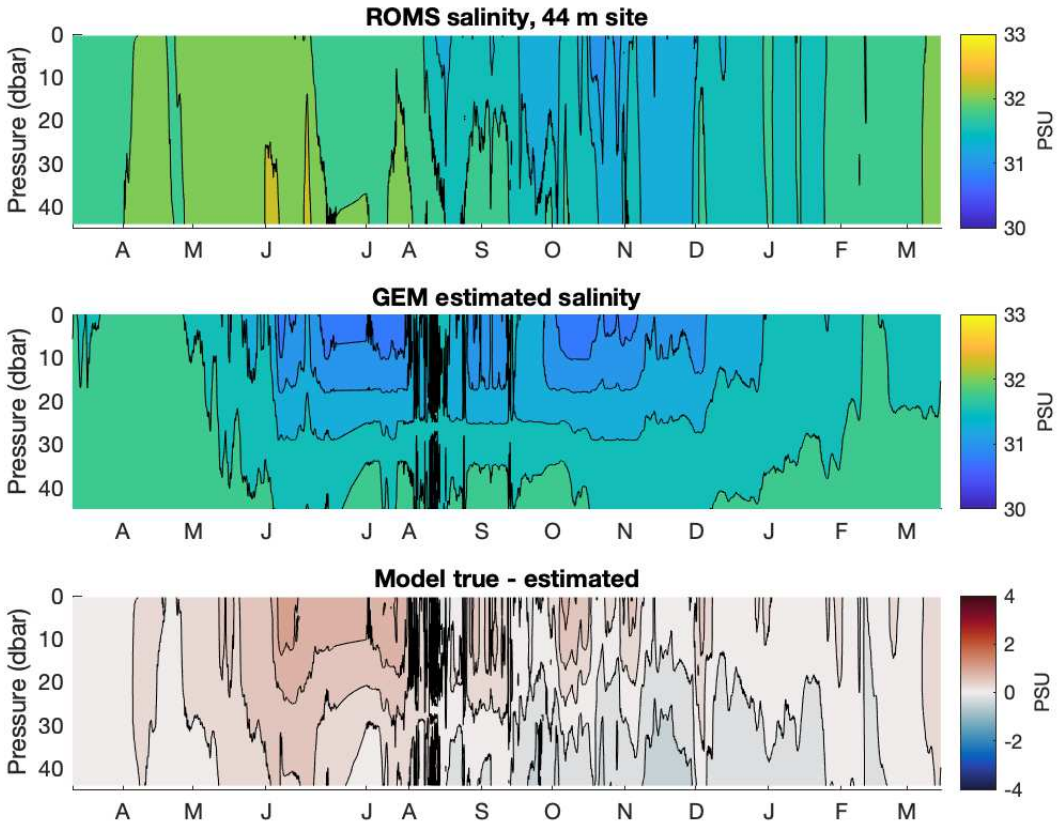

Figure 40. ROMS salinity, GEM estimated salinity, and difference at 44 m site. Contour intervals are 0.25 PSU.

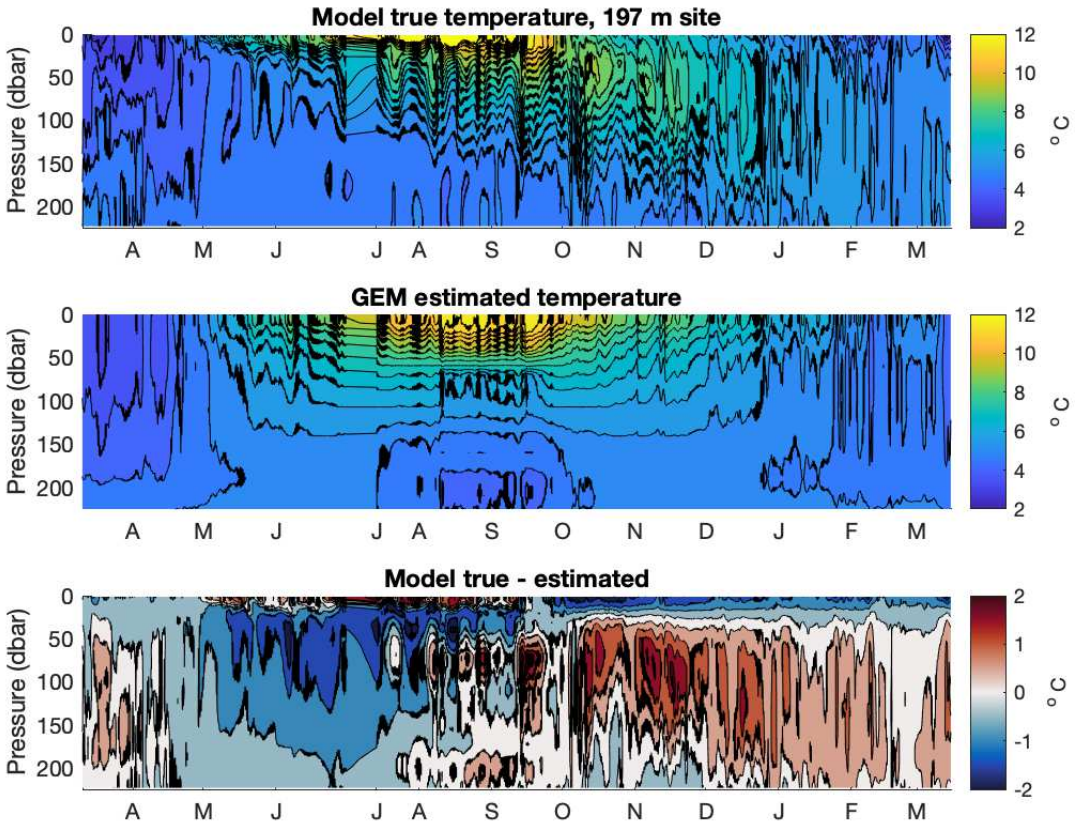

Figure 39. ROMS temperature, GEM estimated temperature, and difference at 197 m site. Contour intervals are 0.5°C.

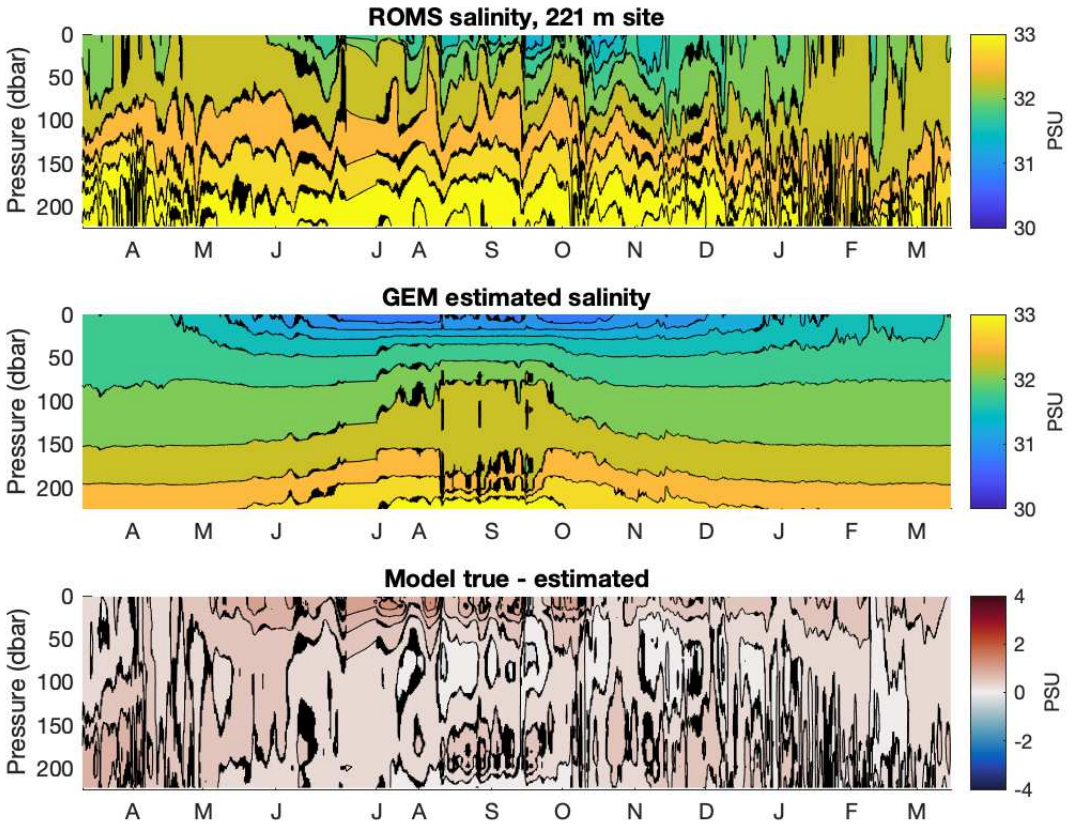

Figure 40. ROMS salinity, GEM estimated salinity, and difference at 197 m site. Contour intervals are 0.25 PSU.

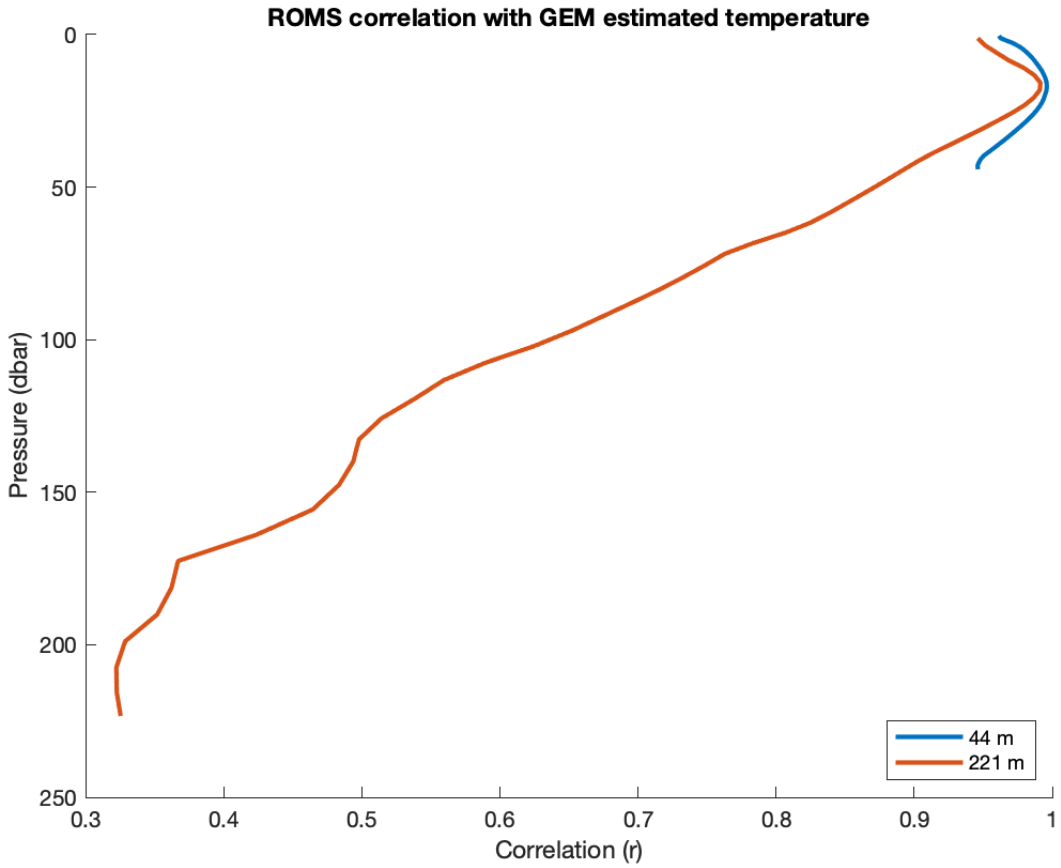

Figure 41. Temporal correlation between ROMS temperature and GEM estimated temperature as a function of depth at each site.

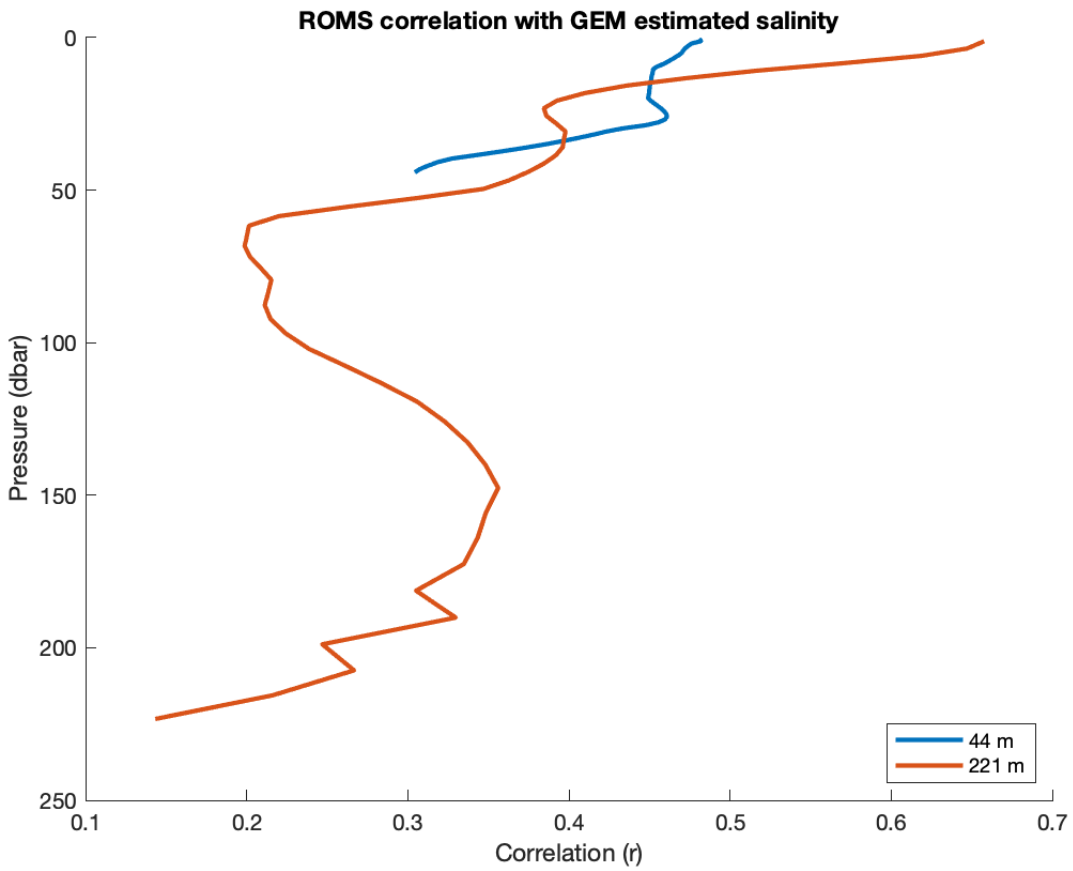

Figure 42. Temporal correlation between ROMS salinity and GEM estimated salinity as a function of depth at each site.

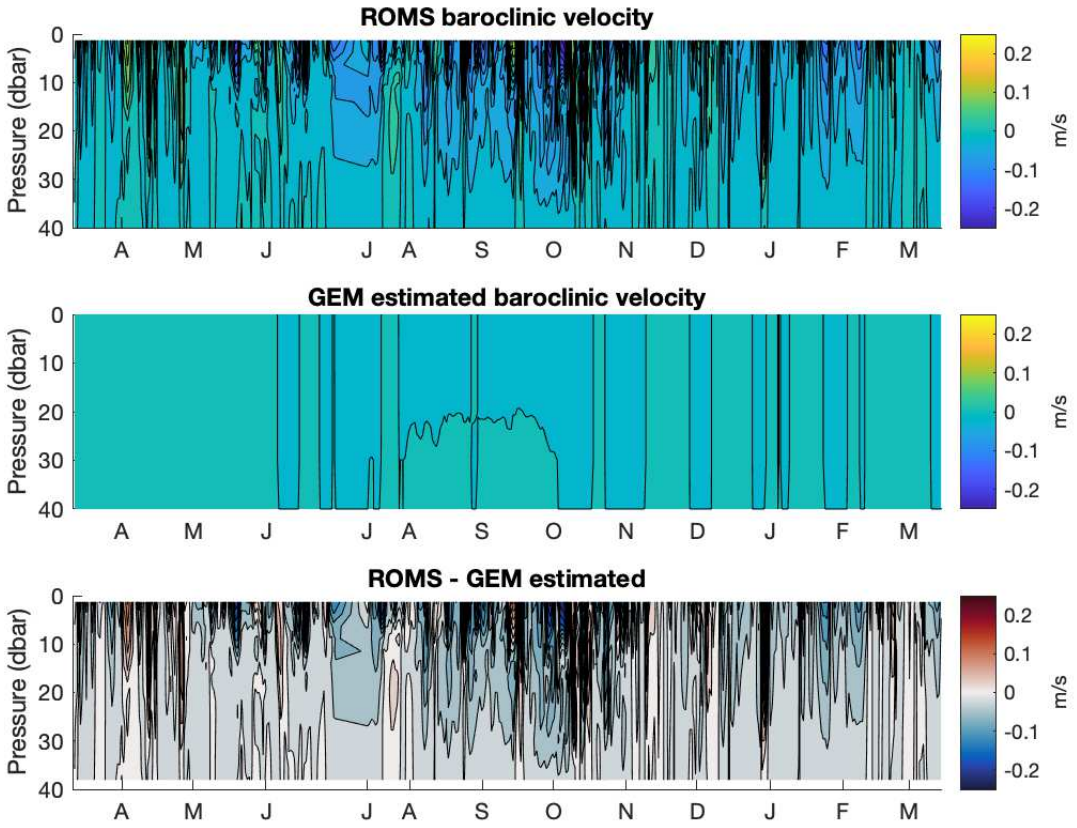

Figure 43. ROMS velocity, GEM estimated velocity, and difference. Contour intervals are 0.1 m/s.

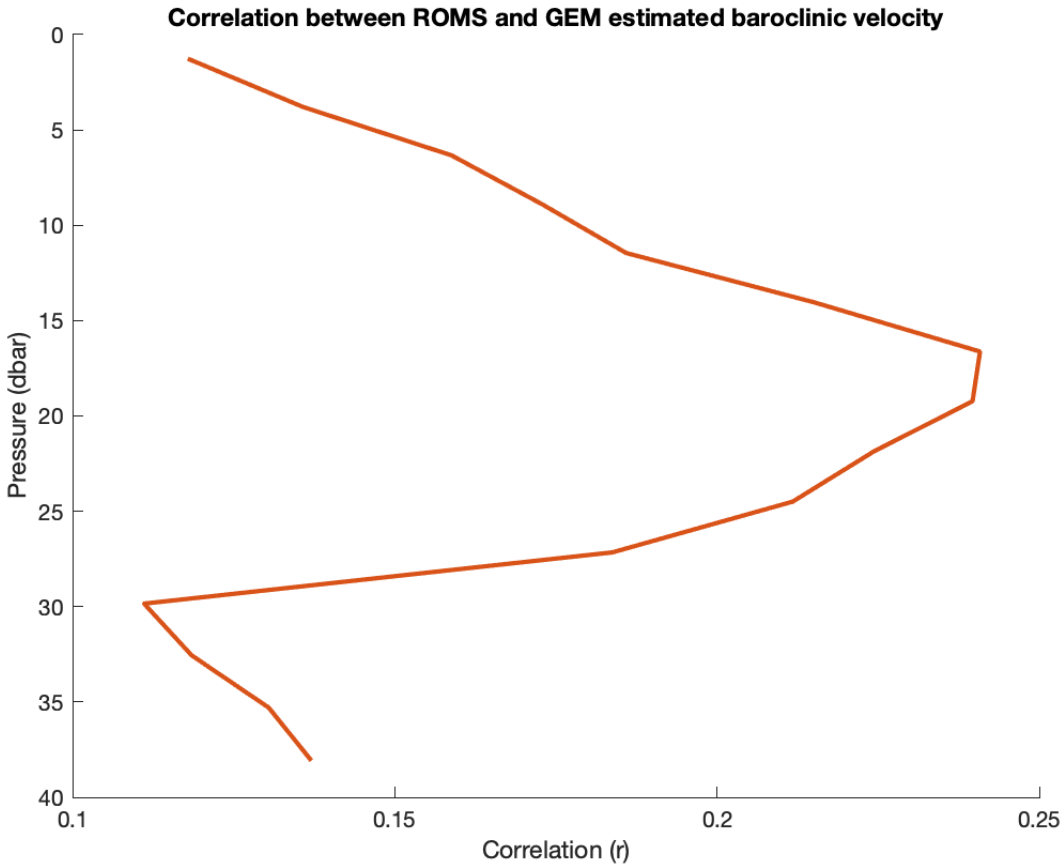

Figure 44. Temporal correlation between ROMS and GEM estimated baroclinic velocity along Shelikof Strait.

6.4 Recommendations

In Shelikof Strait, temperature and salinity are both well estimated by the GEM method. GEMS estimates of baroclinic velocity in Shelikof Strait have lower correlations to the ROMS model than temperature or salinity, however, there is some ability of the GEM estimate to reproduce velocity variability. Deployment of CPIES to monitor flow through the deeper (>200 m) section of Shelikof Strait appears promising.

7 Summary of Recommendations

Signal-to-noise ratios support the theoretical feasibility of using CPIES to estimate profiles of temperature, salinity, and baroclinic velocity on the Beaufort Sea shelf, Lower Cook Inlet, and lower Shelikof Strait. However, salinity errors are sizeable, particularly on the Beaufort Sea shelf and in Lower Cook Inlet. This propagates into large errors in baroclinic velocities in these locations. The large errors in salinity and baroclinic velocity could come from multiple sources. First, it is possible that more CTD profiles would lower errors. This would be worth revisiting in Lower Cook Inlet, as data recovery of historical CTD profiles is currently underway. Second, it is possible that mismatches in location or timing between the ROMS model

and the observed CTD profiles skew our results, but there is no simple way to test this. Third, the relatively weak relationship between salinity and speed of sound (e.g. Figure 1) may make it difficult to use CPIES to estimate salinity in the waters in the Alaska OCS. At latitudes between about 45°S to 45°N, a tight temperature-salinity relationship allows for estimating salinity through its relationship to temperature (e.g. Stewart & Haine, 2016). This is less true at latitudes higher than 45°, such as the Alaska OCS, where salinity is often the dominating source of variability in density. This may present an inherent difficulty in using CPIES on the Alaska OCS.

Despite these challenges, CPIES estimate temperature variance well in Shelikof Strait. Given the relatively shallow depths, a CPIES could be deployed side-by-side with an acoustic Doppler current profiler (ADCP). The ADCP would measure velocity profiles, while the CPIES would estimate temperature and salinity profiles. A test deployment in Shelikof Strait using CPIES owned by BOEM and currently located in Rhode Island is a suggested next step.

8 References

Andres, M., Silvano, A., Straneo, F., & Watts, D. R. (2015). Icebergs and Sea Ice Detected with Inverted Echo Sounders. *Journal of Atmospheric and Oceanic Technology*, *32*(5), 1042–1057. https://doi.org/10.1175/JTECH-D-14-00161.1

Bishop, S. P. (2013). Divergent Eddy Heat Fluxes in the Kuroshio Extension at 144°–148°E. Part II: Spatiotemporal Variability. *Journal of Physical Oceanography*, *43*(11), 2416–2431. https://doi.org/10.1175/JPO-D-13-061.1

BOEM. 2025. Environmental Studies Program Profile: Cook Inlet Physical Oceanography Data Curation, Visualization, and Analyses. Anchorage (AK): U.S. Department of the Interior, Bureau of Ocean Energy Management, Alaska OCS Region. 3 p. [accessed 2025 Mon Day]. https://espis.boem.gov/study%20profiles/BOEM-ESP-AK-22-04.pdf

Coyle, K. O., Pinchuk, A. I., Eisner, L. B., & Napp, J. M. (2008). Zooplankton species composition, abundance and biomass on the eastern Bering Sea shelf during summer: The potential role of water-column stability and nutrients in structuring the zooplankton community. *Deep Sea Research Part II: Topical Studies in Oceanography*, *55*(16), 1775–1791. https://doi.org/10.1016/j.dsr2.2008.04.029

Curchitser EN, Hedstrom K, Danielson S, Kasper J (Rutgers University, New Brunswick, NJ). 2018. Development of a very high-resolution regional circulation model of Beaufort Sea nearshore areas. Anchorage (AK): U.S. Department of the Interior, Bureau of Ocean Energy Management, Alaska OCS Region. 81 p. Report No.: OCS Study BOEM 2018-018. https://espis.boem.gov/final%20reports/BOEM_2018-018.pdf

Danielson, S. L., Weingartner, T. J., Hedstrom, K. S., Aagaard, K., Woodgate, R., Curchitser, E., & Stabeno, P. J. (2014). Coupled wind-forced controls of the Bering–Chukchi shelf circulation and the Bering Strait throughflow: Ekman transport, continental shelf waves, and variations of the Pacific–Arctic sea surface height gradient. *Progress in Oceanography*, *125*, 40–61. https://doi.org/10.1016/j.pocean.2014.04.006

Danielson SL, Hedstrom KS, Curchitser E (University of Alaska, Fairbanks, AK). 2016. Cook Inlet circulation model calculations. Anchorage (AK): U.S. Department of the Interior, Bureau of Ocean Energy Management, Alaska OCS Region. 156 p. Report No.: OCS Study BOEM 2015-050. https://espis.boem.gov/final%20reports/5561.pdf

Danielson S. L., Hennon T. D., Monson D. H., Suryan R. M., Campbell, R. W., Baird, S. J., Holderied, K., & Weingartner, T. J. (2022). Temperature variations in the northern Gulf of Alaska across synoptic to century-long time scales. *Deep Sea Research Part II: Topical Studies in Oceanography*, *203*, 105155. https://doi.org/10.1016/j.dsr2.2022.105155

Donohue, K. A., Watts, D. R., Tracey, K. L., Greene, A. D., & Kennelly, M. (2010). Mapping Circulation in the Kuroshio Extension with an Array of Current and Pressure Recording Inverted Echo Sounders. *Journal of Atmospheric and Oceanic Technology*, *27*, 507–527. https://doi.org/10.1175/2009JTECHO686.1

Dunton, K. H., Weingartner, T., & Carmack, E. C. (2006). The nearshore western Beaufort Sea ecosystem: Circulation and importance of terrestrial carbon in arctic coastal food webs. *Progress in Oceanography*, *71*(2), 362–378. https://doi.org/10.1016/j.pocean.2006.09.011

McMonigal, K., Beal, L. M., Elipot, S., Gunn, K. L., Hermes, J., Morris, T., & Houk, A. (2020). The Impact of Meanders, Deepening and Broadening, and Seasonality on Agulhas Current Temperature Variability. *Journal of Physical Oceanography*, 1–51. https://doi.org/10.1175/jpo-d-20-0018.1

McMonigal, K., Gunn, K. L., Beal, L. M., Elipot, S., & Willis, J. K. (2022). Reduction in Meridional Heat Export Contributes to Recent Indian Ocean Warming. *Journal of Physical Oceanography*, *52*(3), 329–345. https://doi.org/10.1175/JPO-D-21-0085.1

Meinen, C. S., Perez, R. C., Dong, S., Piola, A. R., & Campos, E. (2020). Observed Ocean Bottom Temperature Variability at Four Sites in the Northwestern Argentine Basin: Evidence of Decadal Deep/Abyssal Warming Amidst Hourly to Interannual Variability During 2009–2019. *Geophysical Research Letters*, *47*(18), e2020GL089093. https://doi.org/10.1029/2020GL089093

Peralta-Ferriz, C., & Woodgate, R. A. (2023). Arctic and sub-Arctic mechanisms explaining observed increasing northward flow through the Bering Strait and why models may be getting it wrong. *Geophysical Research Letters*, 50, e2023GL104697. https://doi.org/10.1029/2023GL104697

Rallu De Malibran, M.C., Kaplan, C.M. & Di Lorenzo, E. Marine heatwaves suppress ocean circulation and large vortices in the Gulf of Alaska. *Commun Earth Environ* **5**, 622 (2024). https://doi.org/10.1038/s43247-024-01785-x

Royer, T. C., Vermersch, J. A., Weingartner, T. J., Niebauer, H. J., & Muench, R. D. (1990). Ocean Circulation Influencing the "Exxon Valdez" Oil Spill. *Oceanography*, *3*(2), 3–10.

Sanchez, R., Straneo, F., & Andres, M. (2021). Using Acoustic Travel Time to Monitor the Heat Variability of Glacial Fjords. *Journal of Atmospheric and Oceanic Technology*, *38*(9), 1535–1550. https://doi.org/10.1175/JTECH-D-20-0176.1

Stewart, K. D., and T. W. N. Haine, 2016: Thermobaricity in the Transition Zones between Alpha and Beta Oceans. *J. Phys. Oceanogr.*, **46**, 1805–1821, https://doi.org/10.1175/JPO-D-16-0017.1.

Talley L.D., Pickard G.L., Emery W.J., Swift J.H., 2011. Descriptive Physical Oceanography: An Introduction (Sixth Edition), Elsevier, Boston, 560 pp.

Woodgate, R. A. (2018). Increases in the Pacific inflow to the Arctic from 1990 to 2015, and insights into seasonal trends and driving mechanisms from year-round Bering Strait mooring data. *Progress in Oceanography*, *160*, 124–154. https://doi.org/10.1016/j.pocean.2017.12.007

U.S. Department of the Interior (DOI)
DOI protects and manages the Nation's natural resources and cultural heritage; provides scientific and other information about those resources; and honors the Nation's trust responsibilities or special commitments to American Indians, Alaska Natives, and affiliated island communities.

Bureau of Ocean Energy Management (BOEM)
BOEM's mission is to manage development of U.S. Outer Continental Shelf energy and mineral resources in an environmentally and economically responsible way.

BOEM Environmental Studies Program
The mission of the Environmental Studies Program is to provide the information needed to predict, assess, and manage impacts from offshore energy and marine mineral exploration, development, and production activities on human, marine, and coastal environments. The proposal, selection, research, review, collaboration, production, and dissemination of each of BOEM's Environmental Studies follows the DOI Code of Scientific and Scholarly Conduct, in support of a culture of scientific and professional integrity, as set out in the DOI Departmental Manual (305 DM 3).